

The resonant structure of Jupiter's Trojan asteroids I: Long term stability and diffusion

P. Robutel¹ and F. Gabern²

¹ Astronomie et Systèmes Dynamiques, IMCCE-Observatoire de Paris,
77 Av. Denfert-Rochereau, 75014 Paris, France.

² Departament de Matemàtica Aplicada I, Universitat Politècnica de Catalunya,
Diagonal 647, 08028 Barcelona, Spain.

Abstract

We study the global dynamics of the jovian Trojan asteroids by means of the Frequency Map Analysis. We find and classify the main resonant structures that serve as skeleton of the phase space near the Lagrangian points. These resonances organize and control the long-term dynamics of the Trojans. Besides the secondary and secular resonances, that have already been found in other asteroid sets in mean motion resonance (e.g. Main belt, Kuiper belt), we identify a new type of resonance that involves secular frequencies and the frequency of the Great Inequality, but not the libration frequency. Moreover, this new family of resonances plays an important role in the slow transport mechanism that drives Trojans from the inner stable region to eventual ejections. Finally, we relate this global view of the dynamics with the observed Trojans, identify the asteroids that are close to these resonances and study their long-term behaviour.

1 Introduction

The problem of the stability of the Trojan asteroids has troubled scientist since they were first discovered one hundred years ago. The pioneering work of [Levison et al., 1997] opened a door to a way of studying this problem by performing very long-term dynamical simulations. They encountered that the Trojan swarms are not indefinitely stable and established a one billion (10^9) years stability curve. Later on, [Michtchenko et al., 2001] studied the effect of planetary migration on Jupiter's Trojans and [Nesvorny and Dones, 2002] looked at the hypothetical Trojan population of Saturn, Uranus and Neptune (nowadays, we know that Martian and Neptunian Trojans have been observed). All these studies (and others similar) are based on intensive numerical integrations and performed in the framework of the Outer Solar System (OSS) model, where the influence of the four major planets is taken in consideration.

On the other hand, analytical and semi-analytical studies have provided important results that give insights on the stability problem of the Trojans. These works, mainly based on normal form computations, are generally developed using the Restricted Three-Body Problem [Giorgilli et al., 1989, Simó, 1989, Giorgilli and Skokos, 1997, Gabern et al., 2005, Efthymiopoulos and Sándor, 2005]. Recently, more sophisticated semi-analytical models [Beaugé and Roig, 2001, Gabern and Jorba, 2004] have been used in order to study the stability near the Lagrangian points. Even though these models are not accurate enough to describe realistically the long-term dynamics [Gabern et al., 2004], we believe that these initial works are necessary to develop a general semi-analytical theory of the Trojan Problem.

In spite of all these efforts (and of many others not mentioned here) some fundamental questions remain still open. Besides the stability problem, which is the core of the present paper, questions related to the formation of the Trojans, to the large inclination of some of these asteroids (up to 40 degrees) and to the dynamical differences between L_4 and L_5 are still unsolved. If we have only

very few clues about the last point (see e.g. [Dvorak and Schwarz, 2005, Robutel et al., 2005]), an effective scenario developed by Gomes, Levison, Morbidelli and Tsiganis in 2005 seems to give a reasonable explanation to the formation and inclination problems. Indeed, it is shown for the first time in [Gomes et al., 2005, Morbidelli et al., 2005, Tsiganis et al., 2005a] that the planetary migration is compatible with the hypothesis that the Jupiter’s Trojans are captured just after the crossing of the 1:2 mean motion resonance between Jupiter and Saturn. Moreover, these numerical simulations give a distribution of the Trojans inclination that agrees with the observed one.

In the present paper, we study the global dynamics near the jovian Lagrangian points by means of the Frequency Map Analysis [Laskar, 1990], focusing on the resonant structure of the phase space, or Arnold web. We work on [Robutel et al., 2005], where a preliminary overview of this global resonant structure and its link with the observed Trojans are given. In contrast, here we describe in complete detail this structure and explain its dynamical implications. We make an exhaustive study of all type of resonances relevant in the Trojan problem and classify them into families according to their dynamical sense. Moreover, we link this structure and classification with the long-term dynamics by using one billion years simulations. In this way, we advance in the understanding of the long-term stability question initially tackled by [Levison et al., 1997].

To develop this numerically intensive study, we need a model which is able to reflect the main dynamical structures of the Trojan swarm in the real system (resonant web, stable regions, chaotic zones, etc.), but that remains as simple as possible. This will help us to better understand the mechanisms that generate the instability and, eventually, the ejection of a particular asteroid. As will be later justified, the model involving Sun, Jupiter, Saturn and the asteroid (SJS model) already satisfies these requirements. In Section 2.3, we build this model starting from the Restricted Three-Body Problem (RTBP) by adding, step by step, the different influences of the SJS model on the Trojans. Like that, we are able to understand which resonant structures dominate the phase space dynamics and from which planet action do they come from.

The current study is not just theoretical, as we are also able to place the observed Trojans on the global dynamical pictures. Some of them are trapped in or very close to the identified resonances and this helps to understand the possible future outcome of the actual asteroids.

The paper is organized as follows: In Section 2, we describe the global structure of resonances near L_4 and classify them depending on the type of frequencies involved. We first study the phase space near Jupiter’s plane of motion and afterwards we study the dependence of this structure on the initial inclination. In Section 3, we perform a one billion year simulation of a large number of initial conditions and study the dependence of the stability region and the resonance structure on time. We also describe the generating mechanism of a new type of resonances involving secular frequencies and the one of the Great Inequality. This new type of resonances turns out to be crucial in the transport of asteroids from the inner stable region to the unstable region, possibly leading to ejection. In Section 4, we compute the basic frequencies of the observed Trojans, identify the ones that are close to resonance and perform a long-term study of some of them. Finally, in Section 5, we present the conclusions and outline future work, emphasizing the study of the effects of the planetary migration on the Trojan present population and stability.

2 Global structures of phase space

2.1 Frequency map and fundamental frequencies

In general, the global dynamics of a given system can be obtained by means of numerical simulations and analysing the output data obtained from this simulation. For instance, a global picture in the action space is often obtained using one of the well known Lyapunov exponent family methods [Froeschlé et al., 1997, Cincotta and Simó, 2000, Cincotta et al., 2003, Lega et al., 2003, Skokos et al., 2004]. In this work, however, we use the Frequency Map Analysis [Laskar, 1990, Laskar, 1999] to study the global dynamics of the Lagrangian tadpole region. This method is very useful when the trajectories of the considered system are close to quasi-periodic. Indeed, in the frequency space, it is easier to understand the dynamics. In

particular, the Arnold web appears naturally and it is easy to identify which are the main resonances that organize the global structure. Examples of global maps given by the frequency analysis can be found in studies of the dynamics of particle accelerators [Laskar, 2003], the asteroid belt structure [Robutel, 2005] and the giant planets [Guzzo, 2005].

For the numerical simulations, we use the symplectic integrators of the family $SABA_n$ with an integration step of 1/2 year [Laskar and Robutel, 2001]. The integration is performed in the SJS system during 10 Myr, except for the long-term simulations where we integrate the trajectories for 1 Gyr (see Section 3).

If we assume that the motion of Jupiter and Saturn is quasi-periodic (which is a very natural assumption on the 10 Myr considered here [Laskar, 1990, Robutel and Laskar, 2000]) the orbit of this planetary system lie on a 5-dimensional invariant torus, with fundamental frequencies $(n_5, n_6, g_5, g_6, s_6)$. The two first frequencies are the proper mean motions (frequencies associated to the orbital motion) of Jupiter and Saturn, respectively; while the other three are the secular frequencies (see Table 1).

In these conditions, the motion of the asteroid can be seen as a trajectory of a 3-degrees of freedom Hamiltonian system with 5-dimensional quasi-periodic forcing. This implies that a quasi-periodic trajectory of this system is parametrized by eight fundamental frequencies. Five correspond to the quasi-periodic forcing associated to the fixed frequencies $(n_5, n_6, g_5, g_6, s_6)$, while the remaining three frequencies characterize the dynamics of the Trojan [Jorba and Villanueva, 1997]. These three fundamental frequencies (ν, g, s) are respectively the proper libration frequency (connected to the libration in the 1:1 Mean Motion Resonance (MMR) with Jupiter), the perihelion proper precession frequency of the asteroid and the one corresponding to its node. They are the image of the Frequency Map, which can be defined as (see [Laskar, 1999])

$$F_\theta : (a, e, I) \longrightarrow (\nu, g, s), \quad (1)$$

where (a, e, I) are, respectively, the initial semi-major axis, eccentricity and inclination of the particle. The phase vector $\theta = (\lambda, \varpi, \Omega)$ has the fixed components: $\lambda = \lambda_5 + \pi/3$, $\varpi = \varpi_5 + \pi/3$ and $\Omega = \Omega_5$, where the subscript 5 indicates that the corresponding elliptic phase is the one of Jupiter.

The accurate determination of the fundamental frequencies ν , g and s will allow us to study the dynamical structures of the frequency space by estimating the diffusion rate [Laskar, 1990, Robutel and Laskar, 2001]. Indeed, phenomena associated to resonances become clear in this space (see Fig. 3) and these are quite easy to identify [Robutel et al., 2005]. In addition, the fundamental frequencies can be considered as proper elements and can be used to locate observed Trojans on these global maps [Robutel et al., 2005].

More concretely, we proceed in the following way: The basic frequencies of the two planets are deduced from the quasi-periodic decomposition of the quantities $\gamma_j = a_j e^{i\lambda_j}$ for the proper mean motions n_j , $z_j = e_j e^{i\varpi_j}$ for g_j and $\zeta_j = \sin(I_j/2) e^{i\Omega_j}$ for s_j , where j equals 5 or 6 depending on we are referring to Jupiter or Saturn. These frequencies are reported in Table 1. The proper mean motion of the Trojans is equal to the one of Jupiter because, by definition, the Trojan swarms are in the 1:1 orbital resonance with Jupiter. Thus, the basic libration frequency can be extracted from the decomposition of the function $\gamma = a e^{i(\lambda - \lambda_5)}$. More precisely, if we restrict to a linear secular approximation (see the appendix), Eqs. (32) and (33) show that the semi-major axis and mean longitude of a Trojan can be written as:

$$\begin{aligned} a &= a_5 + d \sin(\theta) + \dots, \\ \sigma &= \lambda - \lambda_5 = \pi/3 + D \cos(\theta) + \dots, \end{aligned} \quad (2)$$

where θ is the libration angle and D the amplitude of libration inside the 1:1 MMR. The quantities d and D are related, at least for small amplitudes of libration [Milani, 1993], by ¹:

$$\frac{d}{a_5} = \sqrt{3\varepsilon} D (1 + O(D^2)), \quad (3)$$

where $\varepsilon \approx m_5/m_0$ and, m_0 and m_5 are, respectively, the Sun and Jupiter masses (see the appendix).

¹A more general relation can be found in [Erdi, 1997]

Table 1: Basic frequencies of the planets in the SJS system. Only the first five frequencies are the fundamental ones (the basis of the quasi-periodic decomposition). The last three frequencies are linear combinations of the proper mean motions: $\nu_{p,q} = pn_5 - qn_6$. We include them in the table because they play a major role in the dynamics of the Trojan swarms.

	frequency ("/yr)	Period (yr)
n_5	109254.63165	11.8622
n_6	43995.34975	29.4577
g_5	4.02760	321780
g_6	28.00657	46274.9
s_6	-26.03912	49771.3
$\nu_{2,5}$	-1467.48545	883.143
$\nu_{1,2}$	21263.93315	60.9482776
$\nu_{1,3}$	-22731.4176	57.0136022

Equations (2) imply that

$$\gamma = a_5 e^{i\pi/3} \left[1 + \frac{1}{2i} \left(\frac{d}{a_5} - D e^{-i\pi/3} \right) e^{i\theta} - \frac{1}{2i} \left(\frac{d}{a_5} + D e^{-i\pi/3} \right) e^{-i\theta} + \dots \right] \quad (4)$$

and thus, in most of the cases (except for very chaotic trajectories), the libration frequency ν is easily extracted from the quasi-periodic decomposition of γ .

The two basic secular frequencies of the Trojan trajectories, g and s , are computed respectively using the analysis of the functions $z = e \exp(i\varpi)$ and $\zeta = \sin(I/2) \exp(i\Omega)$. It is not difficult to recognize the frequency g among the quasi-periodic decomposition of z . Indeed, this frequency takes generally values between 260 "/yr and 430 "/yr [Robutel et al., 2005] and, thus, it is well separated from the planetary secular frequencies (see Table 1). On the other hand, sometimes it is difficult to differentiate the frequency s , that takes values in the interval $[-50 \text{ "/yr}, 10 \text{ "/yr}]$, in the quasi-periodic decomposition of ζ . This is especially true when the considered Trojan moves near the secular resonance $s = s_6$. Even though this can be a problem in the determination of s for a single trajectory, it is not for global studies. Indeed, a few wrong frequencies out of tens of thousands do not affect the global structure.

The Frequency Map allows us to evaluate the diffusion rate of the trajectories. We proceed as follows: The integration and frequency analysis is performed in two consecutive intervals of 5 Myr. In this way, we obtain two different sets of basic frequencies (named, (ν^1, g^1, s^1) for the first interval and (ν^2, g^2, s^2) for the second one). If a given trajectory is quasi-periodic, the two sets of frequencies are identical (up to a given threshold depending on the accuracy of the method). On the other hand, if the trajectory is not quasi-periodic but wanders around tori, a drift on the frequencies is observed and this drift measures somehow the chaoticity of the orbit (how far it is from quasi-periodic motion); see [Laskar, 1999]. Furthermore, we use the relative change of the frequencies,

$$\sigma_\nu = \frac{\nu^1 - \nu^2}{\nu^1},$$

namely *diffusion index* (defined similarly for the other frequencies), as indicator of the regularity of the motion for a particular trajectory. In Fig. 1 we show several global pictures of the diffusion indicator, where we assign a color to $\log \sigma_\nu$. The color scale goes from blue, that corresponds to stable regions

($\sigma_\nu < 10^{-7}$), to red for very chaotic regions ($\sigma_\nu > 10^{-2}$). In black, we display the particles that have been ejected. More details on these plots will be given in the forthcoming sections.

We obtain similar pictures for the diffusion index of the frequencies g and s , although the last one gives slightly larger frequency variations due to the poorer accuracy on the determination of the frequency s (that may need longer integration times).

Of course, one can generate pictures similar to the ones in Fig. 1, draw the resonant structure and have an estimation of the diffusion by using other methods. For example, methods based on Lyapunov exponents [Nesvorný and Dones, 2002] or spectral analysis [Michtchenko et al., 2001] have been used in the past and given similar global pictures, but with much less detail. In the present work, we obtain very high precision global dynamical pictures and, with the aid of the Frequency Map analysis, we are also able to identify and classify the resonances that generate the instability and that govern the long-term diffusion.

2.2 The Sun–Jupiter–Saturn model

We perform our main study using the SJS model. In this section, we aim to justify this particular choice.

The SJS model already captures the main features of the co-orbital region obtained in the (more realistic) OSS model (see Fig. 1). This is explained more in detail in Section 2.3.2. Indeed, the dynamical structures in both models are practically the same (compare Figs. 1.d and 1.e). The SJS model is a restricted four-body problem that includes the main forcing secular frequencies (see [Gabern, 2003, Gabern et al., 2004]), namely the frequencies g_5 , g_6 and s_6 associated to the couple Jupiter–Saturn, but also the short periodic terms associated to the mean motion combinations: n_5 , $\nu_{1,2} = n_5 - 2n_6$, $\nu_{1,3} = n_5 - 3n_6$, and the frequency of the Great Inequality (GI): $\nu_{2,5} = 2n_5 - 5n_6$.

Obviously, given a concrete initial condition, the frequencies associated to the corresponding trajectory (assuming that this orbit is quasi-periodic) in the SJS model are slightly different from the ones in the OSS. But, if we want to compare a particular trajectory of an observed Trojan with its dynamical environment, the global picture is consistent provided that the same model is used for both simulations [Robutel et al., 2005].

Also, for high inclinations, secular resonances with s_7 and s_8 ($s_7 \approx -3$ "/yr, $s_8 \approx -0.7$ "/yr) are of certain importance [Milani, 1993, Tsiganis et al., 2000]. Of course, these resonance do not appear in the SJS model but, again, their relevance is only local and they do not influence in the global dynamical structure which is essentially the same. For instance, in the case of 1868–Thersites, the resonance that causes its ejection from the co-orbital region is $s = s_6$. The resonances involving the frequencies s_7 and s_8 just increase the diffusion speed and help the asteroid to reach rapidly the large chaotic zone associated to the s_6 secular resonance. In the SJS model, the same kind of chaotic behavior is observed but on a larger time scale.

A second reasoning that justifies the use of the SJS model is the following: It is not difficult to deduce, from the secular linear theory given in [Morbidelli, 2002] (see also the appendix), that the contribution of the planet j to the frequency g is equal to

$$\frac{n}{4} \frac{m_j}{m_0} \alpha_j^2 b_{3/2}^{(1)}(\alpha_j), \quad \text{with} \quad \alpha_j = \frac{a}{a_j}, \quad (5)$$

where m_0 corresponds to the mass of the Sun, m_j to the mass of the planet j , n to the mean motion of the particle and $b_{3/2}^{(1)}$ is a Laplace coefficient [Morbidelli, 2002]. For the secular frequency s we have a contribution which is exactly the same with an opposite sign. This computation gives a value of 7.24 "/yr for Saturn, 0.08 "/yr for Uranus and 0.02 "/yr for Neptune. The relative smallness of Uranus' and Neptune's contributions to the frequencies g and s justifies as well that these two planets are not taken into account in a model for the dynamics of the Trojans. In the worst case, we observe that the secular frequencies obtained in the SJS model are slightly shifted (by an amount of the order given above) from the ones obtained with the OSS.

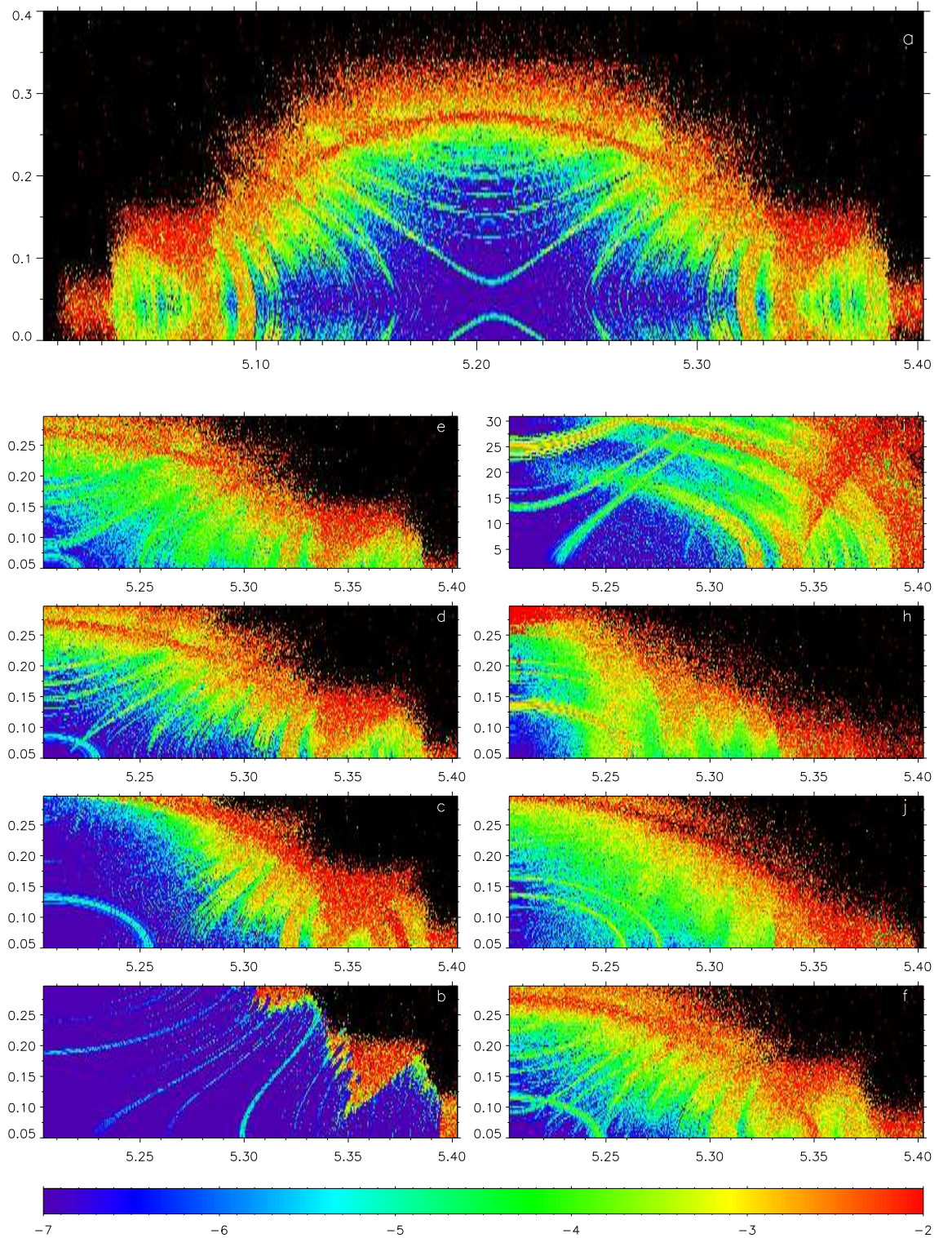


Figure 1: Global pictures of the diffusion index around L_4 . Blue color corresponds to stable regions and red to strongly chaotic motion. The black zone denotes trajectories that lead to ejection before 10 Myr. The axis are (a, e) everywhere except in the (i) frame. In (a) and (d) frames, the diffusion index is computed in the SJS system by fixing the initial inclination to $I = I_5$ and $I = I_5 + 2^\circ$. In the (b), (c) and (e) frames, we use respectively the ERTBP, QPTBP and OSS models and $I = I_5 + 2^\circ$ as initial inclination. The frames (f), (j), (h) and (i) are devoted to study the dependence of the diffusion index on the initial inclination in the SJS model. In particular, we set $I = I_5 + 10^\circ$ in (f), $I = I_5 + 20^\circ$ in (j) and $I = I_5 + 30^\circ$ in (h), and in (i) we fix $e = e_5$ and study the diffusion index in the (a, I) plane. See text for more details.

2.3 Dynamics in Jupiter’s plane of motion

2.3.1 Symmetries in the global pictures

Fig. 1.a shows a dynamical map of the tadpole region of the leading Lagrangian point L_4 . The image is created computing the diffusion index for 70,000 initial conditions and assigning, as explained above, a color code to the corresponding trajectories. The semi-major axis and eccentricities of these initial conditions are taken on an equidistant grid of points belonging to the domain $(a, e) \in [5.005, 5.403] \times [0, 0.4]$. The remaining initial elliptic elements are fixed to: $I = I_5$, $\lambda - \lambda_5 = \pi/3$, $\varpi - \varpi_5 = \pi/3$ and $\Omega = \Omega_5$. This is a natural choice since, in the Elliptic RTBP, these are the elliptic elements of the L_4 point.

This figure shows that, even close to L_4 , there is a web of unstable structures (initial conditions with a diffusion index $\sigma_\nu > 10^{-3}$). But, before studying this resonant structure (this will be done in Section 2.3.2), we want to note that these regions of high diffusion are symmetric. More precisely, we can clearly observe two different type of symmetries.

The first one is a symmetry with respect to the line $a = a_5$ (initial semi-major axis of Jupiter), and it is essentially due to the symmetry with respect to the libration centre. Analytically, this symmetry can be justified easily from the linear secular approximation (35) in the appendix. But, if we look more closely to the picture, we see that actually the axis of symmetry is not exactly the line $a = a_5$ but a curve very close to it. This is due to the non-linear terms and the fact that the libration centre depends on the eccentricity [Nesvorny et al., 2002].

The second symmetry that we observe is the one with respect to the axis $e = e_5$. This symmetry can be explained analytically (in the simpler ERTBP) by Eq. (35), if we remember that in our choice of coordinates $\varpi = \varpi_5 + \pi/3$, and thus $\cos \sigma_g = 1$. Moreover, the fundamental frequencies corresponding to a given initial condition and the ones corresponding to one of its two symmetric points are the same. These frequencies parametrize the KAM torus on which the given trajectories lie. This does not mean that the two corresponding trajectories are the same, but that they lie on the same invariant torus. From the dynamical point of view, these trajectories are equivalent. These symmetries point out the fact that there are manifolds (even close to L_4) where the frequency map is degenerated (see [Gubern et al., 2005]). These symmetries allow us to restrict the sample of initial conditions to the subset $\{(a \geq a_5, e \geq e_5)\}$. This is done in Figs. 1.b–1.h for different models and different initial conditions. In particular, Fig. 1.d corresponds to this subset of initial conditions for the Sun–Jupiter–Saturn model, with initial inclination $I = I_5 + 2^\circ$. Figs. 1.b and 1.c correspond to the simulation in simpler models. Fig. 1.e shows the same type of computation for the OSS model (i.e. taking also in consideration the effects of Uranus and Neptune). All these simulations use small initial inclinations ($I = I_5 + 2^\circ$). Figs. 1.f, 1.g and 1.h correspond to different initial inclinations and Fig. 1.j shows a simulation for the (a, I) plane. For more details, see the forthcoming sections below.

2.3.2 The resonant structure for low inclinations

Here, we describe the dynamics of the tadpole region of the leading Lagrangian point L_4 for small initial inclinations. This particular choice of the slice of initial conditions is not arbitrary at all. Indeed, the dynamical structure is the richest for small inclinations. In particular, the four families of resonances that affect the global dynamics (see below) appear in this slice. The complete description of the resonant structure for low inclination will allow us to understand the main dynamical features for all initial inclination values (see Section 2.4).

In order to identify the resonances associated to the unstable regions and to understand where do they come from, we investigate three different models. The first model is the planar Elliptic RTBP. In a second model, we consider the actual motion of Jupiter in the SJS problem but we neglect the direct effect of Saturn on the Trojan. The third one is our model problem, the Sun–Jupiter–Saturn system. In this way, it is very nice to see how adding new features to the models, new families of resonances appear. In our model, we are able to identify four different families. The first two families correspond to *secondary resonances*: resonances between the proper libration frequency ν and frequencies of the planetary system

(see [Lemaitre and Henrard, 1990] and [Morbidelli, 2002] for more details). The third family contains the secular resonances and the last one is associated to the GI.

Elliptic Restricted Three-Body Problem. The planar Elliptic RTBP (ERTBP) considers the motion of a particle under the influence of Sun and Jupiter, assuming that the motion of the planet is prescribed in a fixed ellipse around the Sun. Despite its simplicity, this time-periodically perturbed two-degrees of freedom problem (where the fundamental frequencies are ν , g and n_5) already contains large chaotic structures. The diffusion index is represented in Fig. 1.b. This figure describes the global dynamics of this problem and shows a very sharp transition from regular (blue) regions to the escaping trajectories zone (in black). Three large unstable regions (yellow to red zones), lying respectively around $(a, e) = (5.32, 0.275)$, $(a, e) = (5.36, 0.175)$ and $(a, e) = (5.4, 0.075)$, penetrate the stable zone from the black outer part. Their shape is very typical of the overlapping of resonant multiplets. For small eccentricities, each resonance of a given multiplet is isolated, while a partial overlapping occurs for larger values of the initial eccentricity (see [Morbidelli, 2002] for details). The phenomenon that generates these unstable regions is easy to understand in the frequency space (see Fig. 2). Indeed, as n_5 is a constant frequency, the frequency space is only two dimensional, and, thus, a single resonance corresponds to a straight line of rational slope in the (ν, g) -plane with equation:

$$p\nu + qg = -k_5 n_5, \quad (p, q, k_5) \in \mathbb{Z}^3. \quad (6)$$

The resonant lines defined by (6) are clearly visible on Fig. 2. This picture shows in frequency space (small black dots) the image of Fig. 1.b by the Frequency Map, $F_\theta : (a_0, e_0) \mapsto (g, \nu)$, and it can be seen as the dual image of that figure. This image is smooth in regular regions, but singularities arise in chaotic zones. Indeed, singularities of the Frequency Map are directly correlated to instabilities of the corresponding trajectories [Laskar, 1999]. To further clarify the relationship between the frequency space and the action space (Fig 1.b), we have superimposed on this figure the labels corresponding to the image of the boundaries of the sample of initial conditions, i.e. $a = a_5$ and $e = e_5$. They correspond to the lower edges of the thin black triangle. The middle vertex of this triangle where black dots accumulate, at about $(g, \nu) = (355, 8825)$, corresponds to the L_4 point. Thus, the boundary of the domain of the frequency map (Fig 1.b) does not correspond to the boundary of the image (Fig. 2). This is due to the fact that the image of the initial domain at (a, e) by the frequency map is folded along a curve where the frequency map is singular (see [Gabern et al., 2005] and [Laskar, 2003]).

The three chaotic regions mentioned above are easily identifiable in Fig. 2. They correspond to the three zones where frequencies gather along straight lines and form a very irregular network. These resonant structures are represented in Fig. 2 by the three families of dashed lines, identified respectively, from top to bottom, by $p = 12, 13$ and 14 :

- $12\nu + qg - n_5 = 0$, $q \in \{8, \dots, 13\}$, at $\nu \sim 8800$ "/yr.
- $13\nu + qg - n_5 = 0$, $q \in \{-4, \dots, 8\}$, at $\nu \sim 8300$ "/yr.
- $14\nu + qg - n_5 = 0$, $q \in \{-3, \dots, 3\}$, at $\nu \sim 7800$ "/yr.

These resonant multiplets overlap when the eccentricity increases to give rise to the main chaotic structures in Fig. 1.b, for, respectively, $a = 5.32$, $a = 5.36$ and $a = 5.4$.

This is very different from the circular RTBP (see [Sandor and Erdi, 2003, Sandor et al., 2002]), where resonances do not generate large chaotic structures. Indeed, due to symmetries (D'Alembert relations), the secondary resonances are not defined by (6) but by:

$$p\nu + k_5(n_5 - g) = 0, \quad (p, k_5) \in \mathbb{Z}^2. \quad (7)$$

Thus, for fixed values of k_5 and p , rather than a one parameter family of resonances, we have only a single resonance. [Deprit et al., 1967] mentions the existence of denominators associated to the resonances $(p, k_5) = (11 : 1), (12 : 1), (13 : 1), (14 : 1)$ during the Birkhoff normalization process. But these terms do not generate any difficulty up to degree 15.

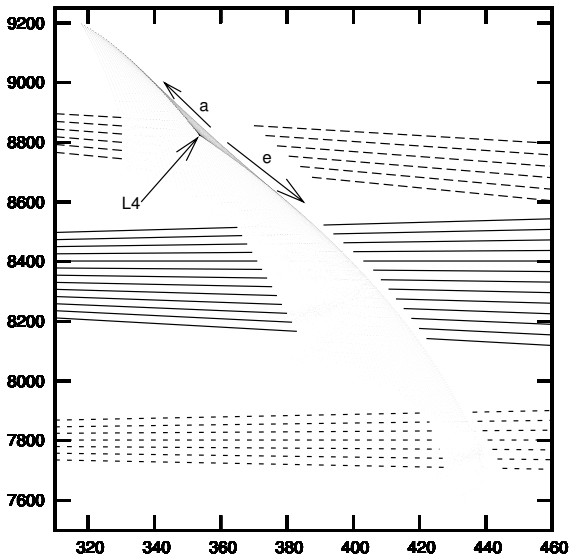


Figure 2: Frequency Map of the ERTBP. Dual image of Fig 1.b in the frequency space (g, ν) . We can see the image of the limit segments of initial conditions ($a = a_5$ and $e = e_5$) as the lower edges of the black triangle with a vertex at about $(g, \nu) = (355, 8825)$. This vertex corresponds to L_4 .

Quasi-Periodic Three-Body Problem. In the second model for the Trojan motion, we consider the influence of Sun and Jupiter on the particle, but now assuming that Jupiter lies in the actual solution of the SJS system. Assuming that Jupiter's motion is quasi-periodic, the system can be described by the 5 fundamental frequencies of the planets: n_5, n_6, g_5, g_6 and s_6 . It is important to point out that in this model, in contrast with the SJS, we disregard the direct effect of Saturn on the particle.

This model is then a restricted Three-Body Problem where the motion of Jupiter is a quasi-periodic motion on a 5D torus. We will call it Quasi-Periodic Three-Body Problem, or QPTBP for short.

In Table 2, we show the 20 terms with larger amplitude of the quasi-periodic decomposition of $z_5 = e_5 \exp(i\varpi_5)$. The two largest terms are associated to the frequencies g_5 and g_6 , that are secular frequencies of the considered planetary system. The rest of the terms, for which the amplitude is 50 to 100 times smaller than the previous ones, are mainly associated to short period arguments, especially $\nu_{1,2}, \nu_{2,5}$ and $\nu_{1,3}$ (see Table 2). The frequency s_6 does not appear in this table, because in the decomposition of z_5 it occupies the twenty-sixth position. As for the quasi-periodic decomposition of the other quantities, i.e. $z_6, \zeta_5, \zeta_6, \gamma_5$ and γ_6 , the leading frequencies are essentially the same, except for ζ_5 and ζ_6 where s_6 is dominant. These additional frequencies that appear in the Quasi-Periodic model will generate new resonances, and eventually new chaotic regions.

Fig. 1.c shows the diffusion index for the QPTBP. Let us start the description of this figure by noticing that the three chaotic structures identified for the ERTBP appear again. They are located at the same place but they are larger than in Fig. 1.b. The first region (the one with $p = 14$ and $a \approx 5.32$) now lies almost entirely in the ejection region (in black). The two other regions are thicker (in the a -direction), but shorter in height due to the shift of the ejection region. This phenomenon arises for, at least, two reasons. First, the new frequencies injected by the quasi-periodic perturbation, in particular the secular frequencies, increase the number of possible resonant harmonics of the secondary resonances. Hence, this type of resonances, that we will call *Family I*, satisfies a more general relation than Eq. (6) defined by

$$\boxed{\text{Family I: } p\nu - n_5 + qg + q_5g_5 + q_6g_6 = 0} \quad (8)$$

with $q + q_5 + q_6 = 1$. For high inclinations, we note that linear combinations of the secular frequencies s and s_6 should be added to this equation.

Table 2: Quasi-periodic decomposition of $z_5 = e_5 \exp i\varpi_5$ in the QPTBP. In the first two columns, we write the amplitudes and frequencies of the frequency analysis. In the last three columns, the decomposition in basic frequencies is shown.

Amplitude	Frequency ($^{\circ}$ /yr)	n_5	n_6	g_5	g_6
4.41×10^{-2}	$+4.027603 \times 10^0$	+0	+0	+1	+0
1.59×10^{-2}	$+2.800657 \times 10^1$	+0	+0	+0	+1
6.44×10^{-4}	-2.126393×10^4	-1	+2	+0	+0
6.28×10^{-4}	$+5.198554 \times 10^1$	+0	+0	-1	+2
3.86×10^{-4}	$+1.411472 \times 10^3$	-2	+5	+0	-2
1.31×10^{-4}	$+2.270341 \times 10^4$	-1	+3	+0	-1
1.05×10^{-4}	-8.652321×10^4	-2	+3	+0	+0
9.92×10^{-5}	$+1.387493 \times 10^3$	-2	+5	+1	-3
8.06×10^{-5}	$+4.399535 \times 10^4$	+0	+1	+0	+0
6.45×10^{-5}	-4.255587×10^4	-2	+4	+0	-1
4.60×10^{-5}	-2.123995×10^4	-1	+2	-1	+1
4.28×10^{-5}	-2.128791×10^4	-1	+2	+1	-1
3.66×10^{-5}	-1.517825×10^5	-3	+4	+0	+0
3.49×10^{-5}	$+7.596451 \times 10^1$	+0	+0	-2	+3
3.45×10^{-5}	$+1.092546 \times 10^5$	+1	+0	+0	+0
2.54×10^{-5}	$+1.435452 \times 10^3$	-2	+5	-1	-1
2.01×10^{-5}	-1.078152×10^5	-3	+5	+0	-1
1.93×10^{-5}	-1.995139×10^1	+0	+0	+2	-1
1.85×10^{-5}	$+2.267943 \times 10^4$	-1	+3	+1	-2
1.82×10^{-5}	$+1.363514 \times 10^3$	-2	+5	+2	-4

The second reason is based on the fact that new families of resonances appear and overlap with the first family. Indeed, Fig 1.c shows two different kinds of new unstable structures: (1) Unstable tongues penetrating the stable region from the escaping zone are visible as yellow to orange straight band structures. These are members of *Family II* (see [Robutel et al., 2005]). And, (2) Two arcs of ellipses centered at the left bottom corner; the largest one in red, bounding the black escaping region, and the other one in light blue close to the left bottom corner. These are members of *Family III*.

The second family of resonances corresponds to a commensurability between the proper libration frequency ν and the frequency $\nu_{1,2}$ mentioned above (see also Table 2). For this reason, we call these resonances: *secondary three-body resonances*. The equation satisfied by this second family is thus

$$\boxed{\text{Family II: } 5\nu - 2\nu_{1,2} + pg + p_5g_5 + p_6g_6 = 0} \quad (9)$$

with $p + p_5 + p_6 = -2$. For small eccentricities, each one of these regions is isolated from the others. But for larger eccentricities, these regions overlap in the border of the stable zone. As we will see below, this border corresponds to a secular resonance and, thus, it belongs to a different family.

It is important to stress that the secondary three-body resonances are not related to the direct action of Saturn (because it is not present in the QPTBP model), but to the short period perturbations of Jupiter's orbit due to Saturn. Instabilities associated to this type of resonances were already mentioned in [Nesvorny and Dones, 2002], and similar effects were found in [Ferraz-Mello, 1997] for a different problem.

We have previously mentioned that the frequencies $\nu_{1,2}$, $\nu_{1,3}$ and $\nu_{2,5}$ play an important role in the temporal evolution of Jupiter's elliptic elements (see Table 2). Actually, the frequency $\nu_{1,3}$ generates

secondary three-body resonances but only for high inclinations (we will see this in Section 2.4). Therefore, we could generalize the second family by adding to Eq. (9) the following relation

$$3\nu + \nu_{1,3} + pg + p_5g_5 + p_6g_6 = 0, \quad \text{with } p + p_5 + p_6 = 2. \quad (10)$$

The frequency corresponding to the Great Inequality, $\nu_{2,5} = -1467$ "/yr, can only generate high order secondary three-body resonances. Indeed, the simplest resonances of this kind that a Trojan can encounter is given by the equation:

$$\nu + 5\nu_{2,5} + pg + p_5g_5 + p_6g_6 = 0, \quad \text{with } p + p_5 + p_6 = 15. \quad (11)$$

But, as we will see later on, the GI plays a key role in the generation of the fourth family of resonances.

The third family of resonances, that already appears in the QPTBP, is the family of *secular resonances*. The most important member of this family is the $s = s_6$ resonance, which is clearly visible in Fig. 1.c as a wide red arch that delimits the region of stability. The importance of this resonance on the study of the stability of the Trojan asteroids was already known more than 25 years ago (see [Yoder, 1979] and [Bien and Schubart, 1984]). It induces very strong instabilities in the neighborhood of the long-term stability zone. Indeed, most of the integrated trajectories that cross this secular resonance escape the libration region before several million years. Many other secular resonances are also present in the co-orbital region. They can be formulated as

$$\boxed{\text{Family III: } qs + q_6s_6 + p_5g_5 + p_6g_6 = 0} \quad (12)$$

with $q + q_6 + p_5 + p_6 = 0$ and $(q + q_6)$ even. For instance, the light blue circular resonance in the bottom-left part of Fig. 1.c (it goes from $e \approx 0.13$ to $a \approx 5.255$), where the diffusion index is of about 10^{-5} , corresponds to the sixth order secular resonance $s - s_6 + g_5 - g_6 = 0$.

As we will see in Section 2.4, secular resonances are more important for high inclinations, except for the $s = s_6$ which dynamical role is more prominent close to the Jupiter's orbital plane (approximately up to 20° of initial inclination).

Restricted Four-Body Problem. The last model is our model example, the Sun–Jupiter–Saturn system, and it was already described in Section 2.2. This is a Restricted Four-Body Problem, since it models the motion of a massless particle that moves under the gravitational influence of three primaries (Sun, Jupiter and Saturn), assuming that these bodies move in the actual solution of the three body-problem.

The global dynamical picture of the co-orbital region corresponding to this model is shown in Fig. 1.d. The new structures that appear in this figure, the thin yellow resonances in the small libration amplitude region (with $a \leq 5.27$), belong to the last family of resonances presented here. These resonances are associated to the GI and, due to their dynamical implications, are one of the most interesting ones:

$$\boxed{\text{Family IV: } pg + \nu_{2,5} + p_5g_5 + p_6g_6 = 0} \quad (13)$$

with $p + p_5 + p_6 = 3$.

These structures, even though they are thin and isolated, are the clue in understanding the slow diffusion process that drive particles from the inner long-term stable region to the escaping zone (see Section 3). Moreover, the dynamical role played by this family of resonances, and to a less extend by the secondary three-body resonances, is enhanced by the fact that some observed Trojans fall very close to these structures and, thus, may be subject to long-term transport phenomena (see Section 4).

Outer Solar System. In Fig. 1.e, we show the global dynamical picture of the co-orbital region for the Outer Solar System (OSS). That is, we study the dynamics of the Trojan asteroids under the influence of the four major planets (Jupiter, Saturn, Uranus and Neptune).

The main structures of this global picture appear already in the SJS model (i.e. in Fig. 1.d), although stronger instability is observed in the inner region and the resonance lines are slightly shifted.

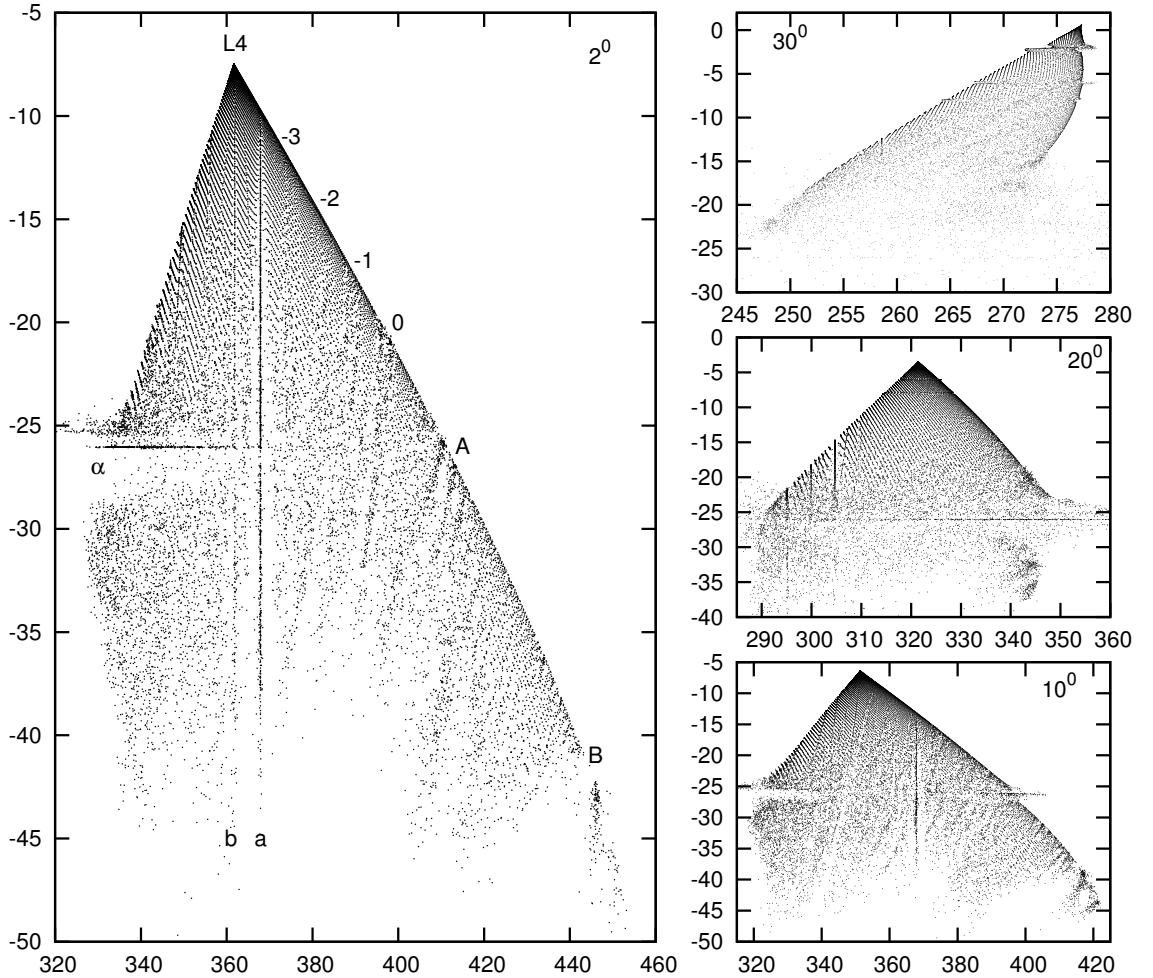


Figure 3: Projection on the (g, s) plane (units: $''/\text{yr}$) of the image of (a, e, I) by the Frequency Map (1) for different initial inclinations. Left: $I = I_5 + 2^\circ$. Right-bottom: $I = I_5 + 10^\circ$, right-centre: $I = I_5 + 20^\circ$ and right-top: $I = I_5 + 30^\circ$. The labels inside the left frame indicate specific resonances belonging to the four different families. See text for more details.

Thus, we believe that the comparison of the main structures in Fig. 1.d and Fig. 1.e clearly shows that the SJS is already a good model to explain the global dynamics of the Sun-Jupiter L_4 tadpole region. This justifies the choice of the main model used in this paper.

Summary: Frequency space. To summarize the families of resonances appearing in the SJS model, we show in Fig. 3 (left) the projection into the (g, s) -frequency space of the image of Fig. 1.d by the Frequency Map (1). It is in this space where resonances are easy to identify and understand.

For instance, the wedges, corresponding to the first family of resonances (8), that appear in Figs. 1.b, 1.c and 1.d are indicated with the labels “A” and “B” in Fig. 3 (left). Respectively, they are generated by (8) with $p = 13$ and $p = 14$.

The secondary three-body resonances are shown in the frequency space with the labels 0 to -3 . These specific numbers correspond to the value of the integer p in the resonance relation (9). Actually, this type of resonances are not isolated but are organized in subfamilies. For each $p = 0, p = -1, \dots, \text{ or } p = -3$, we can see in Fig. 3 as there is an accumulation of thin resonances that are very close to each other. Thus, from now on, when we speak of subfamilies of *Family II*, we will refer to some of the resonances

(9), (10) or (11) for a fixed p value (and for variable p_5 and p_6). The dynamical role of these resonances is important, as the frequencies corresponding to $\nu_{1,2}$, to $\nu_{1,3}$ and to the GI, $\nu_{2,5}$, are associated with terms of large amplitude in the quasi-periodic approximation of Jupiter’s eccentricity (see Table 2).

In Fig. 3 (left), we denote by “a”, the most important representative of the secular family, i.e. $s = s_6$. It is clearly visible as a horizontal line and it corresponds to the border of the stability region (below the $s = s_6$ line, a strong instability is perceived).

The two most representative elements of the last family are associated to the unstable structures denoted by “a” and “b” in Fig. 3. They correspond, concretely, to the resonances

$$4g + \nu_{2,5} + p_5g_5 + p_6g_6 + q_6s_6 = 0,$$

with $p_5 + p_6 + q_6 = -1$.

These are the basic resonant structures that drive the long-term dynamics of the Trojan libration region for low inclinations, that is *Families I, II, III* and *IV* [Robutel et al., 2005]. The role played by the inclination in these structures will be described next.

2.4 Dependence on the initial inclination

In Figs. 1.f, 1.j and 1.h, we show the resonant structure of three slices of the phase space in the (a, e) -plane corresponding, respectively, to initial inclinations $I = I_5 + 10^\circ$, $I = I_5 + 20^\circ$ and $I = I_5 + 30^\circ$. These pictures have been generated in the same way as it was explained in Section 2.3.1. A first obvious conclusion that we can extract from these three figures is that the region from where the Trojans do not escape in less than 10 Myr (non-black region) is practically not affected when we increase the initial inclination up to 20° . For larger inclinations, the stability region starts shrinking when one increases the initial inclination [Gómez et al., 2001, Dvorak and Schwarz, 2005].

The image of these figures by the Frequency Map (see Eq. (1)) can be seen in the three right frames of Fig. 3. From these figures, we are able to easily identify several secular resonances of the type $s = \text{constant}$ (straight horizontal lines): $s - s_6 = 0$, $2s - 3g_5 + g_6 = 0$, $3s - s_6 - 2g_5 = 0$ and $s - s_6 + g_5 - g_6 = 0$. We note that, as the initial inclination increases, the constant term in these secular resonances also increases. For inclinations $I > 20^\circ$, the secular resonance $s = s_6$ disappears from the phase space and therefore, for high inclinations, it does not play any more the crucial role it played in the stability region for low inclinations. This fact may explain why [Marzari and Scholl, 2002] did not find trajectories that, starting near Jupiter’s plane of motion, reached high inclination values. Now, we know that a suitable explanation for the high inclination of the Trojan asteroids orbits might be that they were captured during the early planetary migration process [Morbidelli et al., 2005].

It is not difficult to predict that the effect of the secular resonances associated to the frequency s will increase with the initial inclination I_0 . Indeed, we can see comparing Fig. 1.d with Fig. 1.j and Fig. 1.h that the dynamical significance played by the *Family IV* resonances at low inclinations is replaced at high inclinations by the one of *Family III*.

In Fig. 1.i, we show the resonant structure of the libration region in the (a, I) -plane for a fixed eccentricity $e = e_5$. The most evident structures in this figure are the yellow-to-red archs landing at the a -axis at about 5.32, 5.34, ..., 5.38, etc. The largest one (landing at about $a = 5.38$) corresponds to a subfamily of resonances of the type $3\nu + \nu_{1,3} + pg + p_5g_5 + p_6g_6 + qs + q_6s_6 = 0$, located around $3\nu + \nu_{1,3} - g + g_6 + 2s = 0$. This structure approximately defines the border of the stability region in the (a, I) -plane. Somehow it plays an equivalent role to the one the secular resonance $s = s_6$ did in the plane (a, e) . The arch structure more on the left in Fig. 1.i (the one that lands at about $a = 5.32$) is associated with another subfamily of resonances: $5\nu - 2\nu_{1,2} + pg - (p + p_6 + 2)g_5 + p_6g_6 = 0$.

Actually, all these resonances belong to *Family II*, which has to be generalized, when the initial inclination is not close to Jupiter’s, by including the frequencies s and s_6 . Thus, for high initial inclinations, the relations (9) and (10) satisfied by different subfamilies of *Family II* resonances become respectively:

$$5\nu - 2\nu_{1,2} + pg + p_5g_5 + p_6g_6 + qs + q_6s_6 = 0, \tag{14}$$

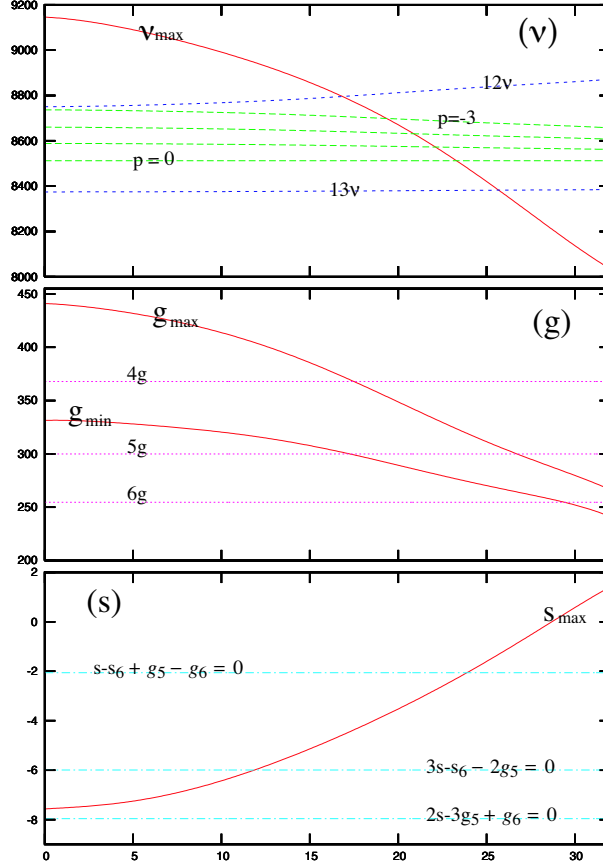


Figure 4: Limit values for the fundamental frequencies of the Trojan asteroids. Top: Maximum values of the libration frequency ν w.r.t. the initial inclination. Centre: Maximum and minimum lines for frequency g w.r.t. the initial inclination. Bottom: Maximum frequency s depending on the initial inclination.

and

$$3\nu + \nu_{1,3} + pg + p_5g_5 + p_6g_6 + qs + q_6s_6 = 0, \quad (15)$$

where $p + p_5 + p_6 + q + q_6 = -2$ in (14), $p + p_5 + p_6 + q + q_6 = 2$ in (15) and $(q + q_6)$ is even.

Similarly, as we increase the inclination, the resonance relations corresponding to *Family IV* (13) should be generalized in order to include the secular frequencies s and s_6 :

$$pg + \nu_{2,5} + qs + p_5g_5 + p_6g_6 + q_6s_6 = 0, \quad (16)$$

where $p + q + p_5 + p_6 + q_6 = 3$ and $(q + q_6)$ even.

In order to understand the transition between the resonances that organize the phase space for different initial inclinations, it is important to mention that the range of frequencies reachable for ν , g and s inside the tadpole region strongly depends on this initial inclination. The upper red lines in the three frames of Fig. 4 correspond to the maximum reachable values for the ν , g and s frequencies depending on the initial inclination. The middle frame also shows the line corresponding to the minimum value for g ².

Moreover, in the top frame of this figure we display *Family I* resonances (the upper blue line corresponding to resonances of the type 12ν and the lower one to 13ν , recall Eq. (8)) and *Family II* resonances (green lines, from bottom to top respectively with $p = 0$ to $p = -3$ in (9)). In the bottom frame of Fig. 4,

²It is clear from Fig. 3 that we cannot define a minimum value for the frequency s , but we can none the less assert that all s values grow with the initial inclination.

the three blue lines correspond to the following members of the *Family III* secular resonances (from top to bottom): $s - s_6 + g_5 - g_6 = 0$, $3s - s_6 - 2g_5 = 0$ and $2s - 3g_5 + g_6 = 0$.

From the middle frame of Fig. 4, it is clear that the fundamental frequency of the longitude of the perihelion of the Trojans g ranges approximately from 330 "/yr to 440 "/yr for small inclinations. We know that the frequency related to the Great Inequality is approximately $\nu_{2,5} = -1467$ "/yr. Thus, the simplest resonances involving g and $\nu_{2,5}$ are of the form: $4g + k_5g_5 + k_6g_6 + \nu_{2,5} = 0$ with $k_5 + k_6 = -1$ (upper pink line in the centre frame of Fig. 4 labeled $4g$, $5g$ and $6g$). For higher inclinations the values of g decrease, and thus resonances involving $5g$ (middle pink line) and even $6g$ (lower pink line) can be reached. It is clear from Fig. 4 that when the resonances involving $4g$ exit the phase space, at about $I = 18^\circ$, the resonances involving $5g$ start playing a role. These ones reach the maximum g value line, at about $I = 27^\circ$, and soon afterwards, at about $I = 29^\circ$, the resonances involving $6g$ enter the phase space. In general, commensurabilities of the type (16) are found for moderate to high inclinations, but have a smaller dynamical influence than the previous ones (see Tables 3 and 8).

3 Long-term dynamics

3.1 Stable region in a one billion years simulation

In Fig. 5, we look at the dependence on time of ejected particles (black zone) in a long (10^9 yr) integration. The initial conditions in the white triangle on the left-bottom corner of every figure are not integrated since we know beforehand that they will not escape during the one billion years simulation. The percentage appearing inside the white triangles indicate how many particles, among the ones that escape in the 1 Gyr integration, have already escaped at a previous given time (this time is written down in Myr in the top-right corner of every figure). It is already known that this dependence of the number of escaped particles w.r.t. time is by no means linear [Simó et al., 1995, Grazier et al., 1999a, Grazier et al., 1999b]. The colored part of the figure is generated in the same way as Fig. 1. That is, for non-escaped particles, we plot the diffusion index corresponding to the first 10 million years of integration. This is actually fine since, if the particle does not escape, the degree of diffusion in the one billion years simulation is very well approximated by the one corresponding to the first 10 Myr. What really makes a qualitative difference is whether the particle is ejected from the stability region or not.

A first look at these pictures tells us that almost all Trojans in a neighborhood of the resonance $s = s_6$ and above are ejected in less than one billion years. Thus, it is again verified the well-known fact that this secular resonance bounds the long-term stability region for low initial inclination values.

A second comment is that we can clearly see the appearance of a big (black) gap around the *Family IV* resonance $4g + \nu_{2,5} - g_5 = 0$ (see top-right frame of Fig. 5 at about $(a, e) = (5.28, 0.15)$). This suggests that this type of resonances may play an important role in a slow diffusion process leading particles from the inner (blue) stable region to the unstable region. We pursue this first impression in Section 3.2, where we study in depth this diffusion mechanism.

Finally, we note that all the initial conditions that have a diffusion index greater than 10^{-3} in the first 10 million years lead to an escaping trajectory, except for two regions related to resonances belonging to two subfamilies of *Family II* (Eq. (9) with $p = 0$ and $p = -1$). In these regions, a strong bounded diffusion transversal to the secondary three-body resonances can be observed. This will be studied in more detail in Section 3.3.

3.2 The role of Family IV

The secondary resonances, like the members of *Family II*, appear frequently when studying asteroidal or Kuiper belt objects in mean motion resonance. A secondary three-body resonance was first mentioned by Ferraz-Mello inside the 2:1 Kirkwood gap (see [Ferraz-Mello, 1997, Ferraz-Mello et al., 1998b, Ferraz-Mello et al., 1998a], and also in chapter 11 of [Morbidelli, 2002]). But in these cases, contrarily to what happens for the resonances of *Family IV*, the commensurability involves the libration frequency ν and the frequency of the GI, $\nu_{2,5}$, (or, eventually, ν and $2n_7 - n_8$ in the Kuiper belt). As far as we

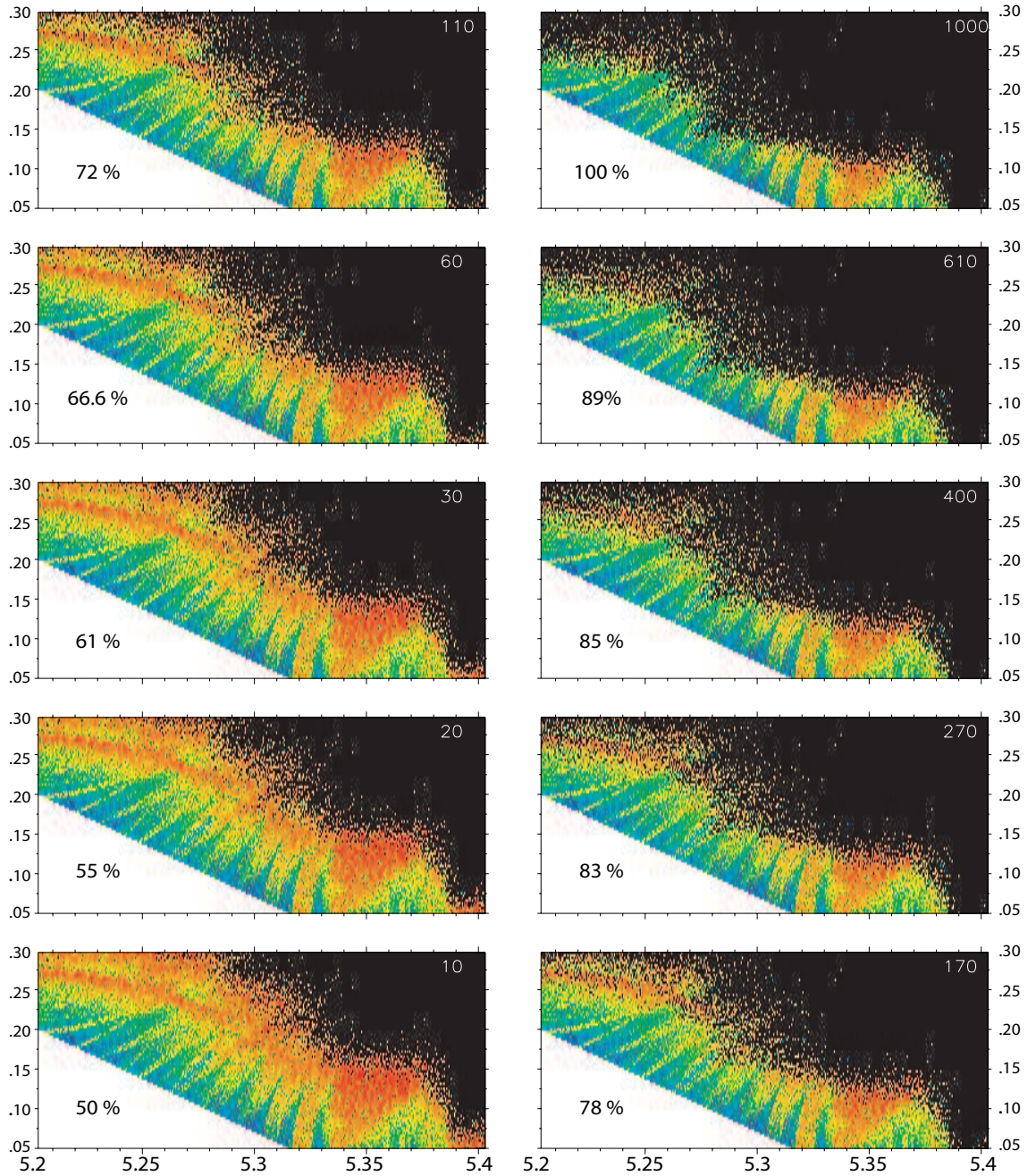


Figure 5: Fraction of ejected particles (black zone) depending on time up to 1 Gyr. The final time for each frame is written (in Myr) in the top-right corner of every figure. The initial conditions inside the white triangles are not integrated since we know beforehand that they will not escape before 1 Gyr. See text for more details.

Table 3: Main *Family IV* resonances of the form $pg + qs + p_5g_5 + p_6g_6 + q_6s_6 + \nu_{2,5} = 0$. For the multiplets that have $q = 0$, we show in the last but one column the corresponding value of the frequency g in "/yr. In the last column, we display the approximate value of the inclination (in degrees) for which the related resonances are achieved.

p	q	p_5	p_6	q_6	g	I
4	0	-1	0	0	367.87	0
4	0	0	-1	0	373.87	0
4	0	-2	1	0	361.88	0
4	-2	1	0	0		0
4	-2	0	1	0		0
5	0	0	-2	0	304.70	20
5	0	-1	-1	0	299.90	20
5	0	-2	0	0	295.11	20
5	-1	0	-2	1		20
6	0	0	-3	0	258.58	30

know, it is the first time that a resonance which is neither purely secular nor secondary (in the sense that ν is not involved) is identified playing a no-negligible dynamical role. Even though the effect of *Family IV* is not dominant in the current configuration of the Solar System, they are involved in the chaotic behavior of some observed Trojans (see Section 4). Above all, the slow diffusion along these resonances and their connection with the secular resonance $s = s_6$ generates a transport mechanism that drives some Trojans from the inner part of the tadpole region to the horseshoe domain, and possibly leading the asteroid to ejection (see Section 3.2.2). Moreover, as it is shown in [Robutel and Bodossian, 2006], if Jupiter and Saturn were closer to the 2:5 mean motion resonance than they actually are, the role played by the resonances of *Family IV* would be dominant.

3.2.1 On the generating mechanism of *Family IV*

We are now going to show how these "unusual" resonances are generated. The first clue is that *Family IV* is due to the direct contribution of Saturn on the Trojan. This was seen in Section 2, where recall that every action on the asteroid of the SJS system was added one at a time. Consequently, we have to focus on the inverse of the mutual distance between the Trojan and Saturn. The elements of the expansion of this term of the Hamiltonian that bring the main contribution to *Family IV* are given by the following expression (and the corresponding complex conjugate):

$$z^\alpha \bar{z}^{\bar{\alpha}} z_6^{\alpha_6} \bar{z}_6^{\bar{\alpha}_6} \exp \{i(2\lambda - 5\lambda_6)\}, \quad (17)$$

where $z = e \exp i\varpi$, $z_6 = e_6 \exp i\varpi_6$ and $(\alpha, \bar{\alpha}, \alpha_6, \bar{\alpha}_6)$ are positive integers satisfying $\alpha - \bar{\alpha} + \alpha_6 - \bar{\alpha}_6 = 3$. Denoting $\zeta = e^{i\sigma}$, (17) becomes:

$$z^\alpha \bar{z}^{\bar{\alpha}} z_6^{\alpha_6} \bar{z}_6^{\bar{\alpha}_6} \zeta^2 \exp \{i(2\lambda_5 - 5\lambda_6)\}. \quad (18)$$

Table 4: Ten first terms of the quasi-periodic approximation of $z = e \exp(i\varpi)$ for a body inside the resonance $4g - g_5 + \nu_{2,5} = 0$. The first column gives the modulus of the complex amplitude of the coefficients divided by $\alpha_0 = 5.9510 \times 10^{-2}$. The frequencies (in "/yr) are given in the second column. In the last column, we show the linear combinations of the main frequencies, where $\nu_l = 1.12971$ "/yr denotes the frequency of libration.

$ \alpha_j/\alpha_0 $	ν_j ("/yr)	combinations
1	367.87821	g
0.719872	4.02760	g_5
0.273389	28.00657	g_6
0.144094	366.74844	$g - \nu_l$
0.0882167	369.00817	$g + \nu_l$
0.016275	109254.63165	n_5
0.0143341	1071.60052	$-g - g_6 - 2\nu_{2,5}$
0.0130212	51.98555	$-g_5 + 2g_6$
0.0111994	731.72892	$2g - g_5$
0.0109928	365.61696	$g - 2\nu_l$

If we assume that the considered trajectories are quasi-periodic, and if we keep only the dominant terms of the composition, we have³:

$$\begin{aligned}
z_5 &= \alpha_{5,5} e^{ig_5 t} + \alpha_{5,6} e^{ig_6 t} + \dots, \\
z_6 &= \alpha_{6,5} e^{ig_5 t} + \alpha_{6,6} e^{ig_6 t} + \dots, \\
z &= \alpha_0 e^{igt} + \alpha_5 e^{ig_5 t} + \alpha_6 e^{ig_6 t} + \dots, \\
\zeta &= \beta_0 + \beta_{-1} e^{-i\nu t} + \beta_1 e^{i\nu t} + \dots, \\
\lambda_5 &= \lambda_5^0 + n_5 t + \dots, \\
\lambda_6 &= \lambda_6^0 + n_6 t + \dots.
\end{aligned} \tag{19}$$

By substitution of (19) into (18), we obtain a sum of monomials which frequency is equal to:

$$n\nu + pg + p_5 g_5 + p_6 g_6 + \nu_{2,5} \tag{20}$$

with $p + p_5 + p_6 = 3$. This expression leads to secondary three-body resonances comparable to the ones that generate *Family II*. But, as the ratio $\nu/\nu_{2,5}$ is close to 13, the value of (20) can never be close to zero (except for unrealistic (high) values of the integers p , p_5 and p_6). However, $n = 0$ gives rise to a resonant combination (with relatively small integer coefficients) belonging to *Family IV* (see Table 3).

Once we know where these resonances come from, it is easy to define a critical angle (an angle that librates inside the considered resonance and circulates outside). To this end, let us consider the particular resonant relation (the generalization to any resonance of *Family IV* will be obvious later on)

$$4g - g_5 + \nu_{2,5} = 0. \tag{21}$$

In this situation, the natural candidate to be the critical angle is

$$\theta = 4\varpi - \varpi_5 + 2\lambda_5 - 5\lambda_6. \tag{22}$$

But, in general, this angle does not librate even very deep inside the resonance (see Fig. 6 (top)). A rigorous way to construct a critical angle is to begin by reducing the Hamiltonian to a normal form, i.e. a Kolmogorov normal form in the neighborhood of the frequencies $(\nu, g, s, g_5, g_6, s_6, \nu_{2,5})$, and to stop the

³See Tables 1, 2 and 4, and more generally [Laskar, 2005], for quasi-periodic representations of planetary solutions.

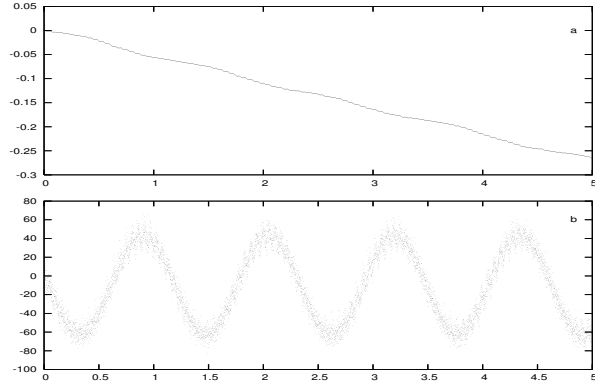


Figure 6: Study of the critical angle of the resonance $4g - g_5 + \nu_{2,5} = 0$. Top: Naïve candidate of critical angle. $4\varpi - \varpi_5 + 2\lambda_5 - 5\lambda_6$ (in millions of degrees) vs time (in Myr). Bottom: Actual critical angle. Argument of $\tilde{z}^4 \exp i(\nu_{2,5} - g_5)t$ in degrees vs time.

process at the step just before eliminating the term that has the divisor corresponding to this resonance (see [Morbidelli, 2002], chapter 11). This procedure, though, is very technical and to perform such a computation would be far from the scope of the present paper. However, an easy way to produce an approximate critical angle is to perform the zero order step of the previous normalization process. This corresponds, in some sense, to diagonalize the quadratic part of the secular Hamiltonian [Laskar, 1990]. In particular, in the first step of the normalization process, we can write (from the third equation of (19)):

$$\tilde{z} = \alpha_0^{-1}(z - \alpha_5 z_5 - \alpha_6 z_6). \quad (23)$$

The following example shows that the transformation (23) is necessary in order to find an approximation of the critical angle. Let us take a fictitious Trojan evolving inside the considered resonance. We pick an initial condition in Fig. 1 such that the corresponding frequencies satisfy approximately (21): $a_0 = 5.2595$, $e_0 = 0.1125$, $I = I_5$, $\lambda = \lambda_5 + \pi/3$, $\varpi = \varpi_5 + \pi/3$ and $\Omega = \Omega_5$. The 10 first terms of the quasi-periodic decomposition of $z = e \exp(i\varpi)$ are given in Table 4. Even though for this body, the proper frequency g satisfies (21), the angle θ defined by Eq. (22) does circulate (see Fig. 6 (top)). As

$$z = \alpha_0 e^{igt} + \alpha_1 e^{ig_5 t} + \alpha_2 e^{ig_6 t} + \alpha_3 e^{i(g-\nu_1)t} + \alpha_4 e^{i(g+\nu_1)t} + \dots, \quad (24)$$

the dominant terms of the quasi-periodic approximation of

$$w(t) = (z(t))^4 e^{-ig_5 t} e^{i\nu_{2,5} t} \quad (25)$$

are given by the complex function of time

$$w(t) = \alpha_0^4 \left(\gamma_1 e^{2i(g_5 - g)t} + \gamma_2 e^{i(g_5 - g)t} \right) \quad (26)$$

with $|\gamma_1| \approx 3.21$ and $|\gamma_2| \approx 3.17$. Then, the argument of w does not librate as it is shown in Fig. 6, but circulates. Contrarily, if we suppress the terms in z containing g_5 and g_6 (this is approximately what we do by computing \tilde{z}), we have:

$$(\tilde{z}(t))^4 e^{i(\nu_{2,5} - g_5)t} = 1 + \delta_{-1} e^{-i\nu_{2,5} t} + \delta_1 e^{i\nu_{2,5} t} + \dots, \quad (27)$$

where $|\delta_{-1}| + |\delta_1| < 1$. If the modulus of the neglected quantity in (27) is small enough (which is the case here), the argument of $(\tilde{z}(t))^4 e^{i(\nu_{2,5} - g_5)t}$ is the critical angle and librates inside the corresponding resonance (see Fig. 6 (bottom)).

3.2.2 Diffusion along Family IV resonances

In Fig. 7 (first two rows), we show different examples of fictitious Trojans that evolve in frequency space following some resonances belonging to *Family IV*. The base for the four figures (black dots) is the same: it is the projection onto the (g, s) -space of the image of the frequency map. On this base, we display (in red) the evolution of the fictitious particles. That is, we choose some particular initial conditions (blue triangles) close to the resonance $4g + \nu_{2,5} - g_5 = 0$ (label “a” in Fig. 3), compute their basic frequencies every 5 Myr and plot them on the figures. We stop the integration at 1 Gyr or when the particle is ejected.

More concretely, in the top-left figure an example of a particle that remains trapped inside the resonance for the whole simulation is shown. The top-right frame of Fig. 7 shows an example of a particle that evolve inside the resonance $4g + \nu_{2,5} - g_5 = 0$ for the first 600 Myr while its s frequency slowly decreases, then it wanders near the upper part of the $s = s_6$ resonance, it finally crosses it and at about 800 Myr it is ejected from the stable region. The third and fourth examples (second row frames of Fig. 7) correspond to particles that leap between the resonances $4g + \nu_{2,5} - g_5 = 0$ and $4g + \nu_{2,5} - 2g_5 + g_6 = 0$. The one in the centre-left figure does not escape during the one billion years simulation, while the fictitious trojan of the centre-right figure is ejected from the stability region after about 800 Myr of integration time.

3.3 Diffusion transversal to Family II resonances

As we mentioned in Section 3.1, all initial conditions in Fig. 5 that have a diffusion index larger than 10^{-3} lead to escaping trajectories, except the ones that belong to a subfamily of the secondary three-body resonances $5\nu - 2\nu_{1,2} + pg + p_5g_5 + p_6g_6 = 0$ with $p = 0$ and $p = -1$ (they correspond to the resonances with labels 0 and -1 in Fig. 3). Thus, a Trojan starting its long-term simulation near one of these resonances is likely to suffer a strong diffusive (since its diffusion index is large) but bounded motion (because it does not escape the tadpole region).

To study in depth this phenomenon, we picked convenient initial conditions near the resonance $5\nu - 2\nu_{1,2} + 0g + 0g_5 - 2g_6 = 0$, integrated them for 1 Gyr, compute their basic frequencies every 5 Myr and look at the time evolution of these frequencies. In the last bottom row of Fig. 7, we show two examples of these integrations. More concretely, the small red dots denote the evolution of the frequencies (g, ν) during the simulation and the green horizontal lines correspond to members of the subfamily of the secondary three-body resonance $5\nu - 2\nu_{1,2} + 0g + qg_5 - (q+2)g_6 = 0$, for $q \in \{-5, \dots, 0, \dots, 4\}$. These particles suffer a strong bounded diffusion in ν and jump randomly from one member of the subfamily of resonances to another, giving a global view of diffusion transversal to the secondary three-body resonances. This type of diffusion is very different from the one generated by *Family IV* and it reminds the Chirikov diffusion mechanism [Chirikov, 1959, Chirikov, 1960].

4 Analysis of the observed Trojans

We are now interested in relating the observed Trojans with the global dynamical maps (Fig. 1), in identifying actual asteroids in the resonances described in Section 2 and in studying the long-term evolution of some of these objects. In this regard, we obtained from [Bowell,] the osculating elliptic elements of the known Trojan asteroids at the Julian date 2452200.5 (October 10th, 2001) to be used as initial conditions for the simulations.

4.1 Inversion of the Frequency Map and Resonant Trojans

In [Robutel et al., 2005], we described in detail an approximated method for inverting the Frequency Map (FM) that allowed us to place the observed Trojans in global pictures similar to the ones in Fig. 1. The problem of inverting the FM resides in the fact that generically all Trojans have different initial phases θ (see Eq. (1)) and the global portraits have just been computed for a particular constant initial phase. To solve this problem, we computed the basic frequencies of the actual Trojans and looked for the closest

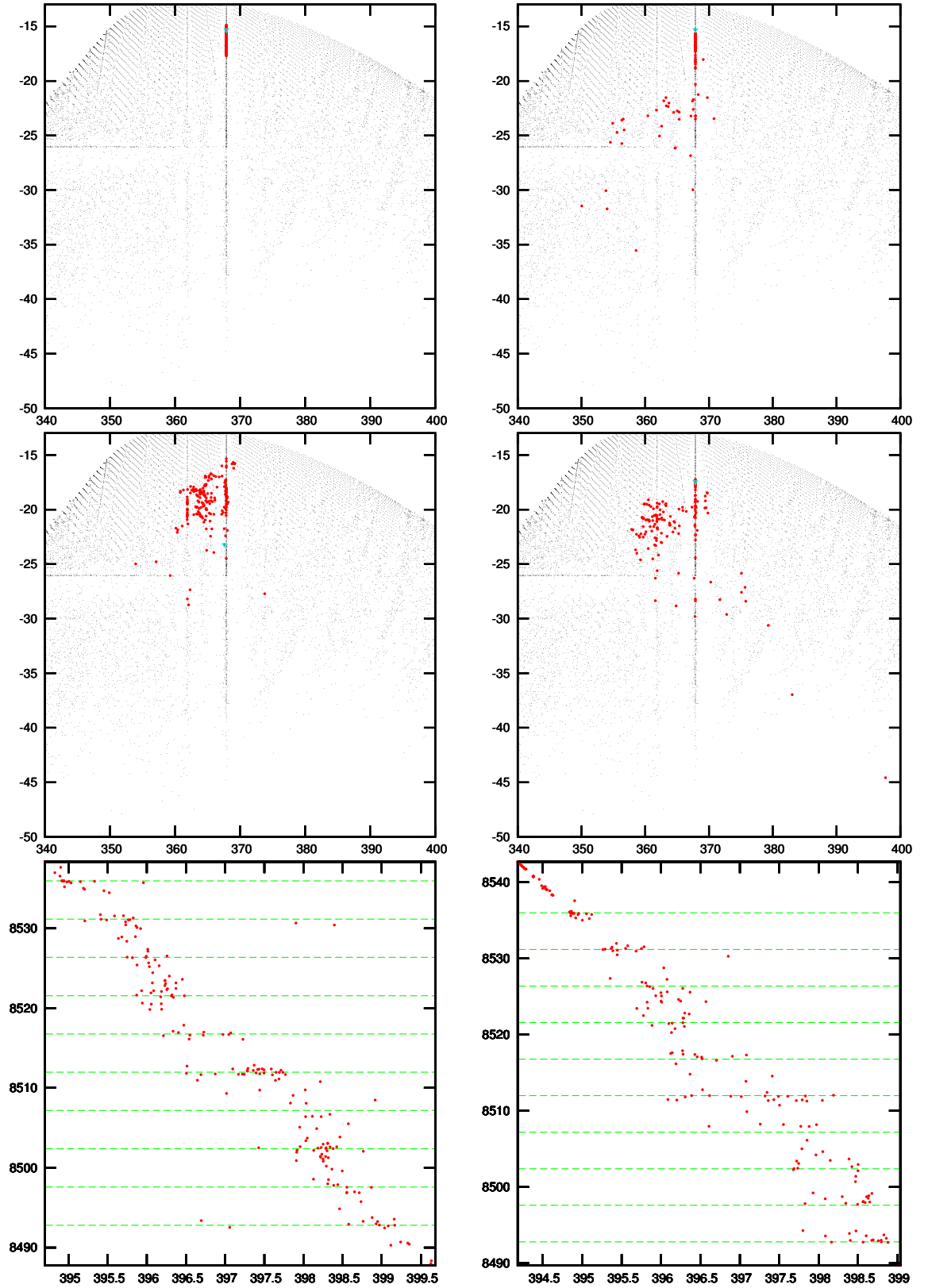


Figure 7: First two rows: Diffusion along *Family IV* resonances of some fictitious Trojans. Long-term evolution of the (g, s) frequencies (red dots) for four different initial conditions (blue points) close to the resonance $4g + \nu_{2,5} - g_5 = 0$. We superimpose this evolution on the image of the global frequency map (Fig. 1). Bottom row: Two fictitious examples of diffusion transversal to the secondary three-body resonances $5\nu - 2(n_5 - 2n_6) + 0g + qg_5 - (q+2)g_6 = 0$, for $q \in \{-5, 4\}$. See text for more details.

Table 5: **Family I.** Actual Trojans at a distance smaller than 0.1 "/yr of a resonance of the type $p\nu - n_5 + qg + q_5g_5 + q_6g_6 = 0$. In the last two columns, we write the asteroid's initial inclination (in degrees) and the distance to the exact resonance (in "/yr).

$p\nu - n_5 + qg + q_5g_5 + q_6g_6 = 0$						
Trojan	p	q	q_5	q_6	I	dis.
1749–Telamon	13	-12	3	10	6.8	0.024
5259–Epeigeus	13	-12	6	7	14.9	0.023
20739–1999XM193	13	-13	4	10	13.4	0.004

initial condition in the global picture that had the same image by the FM. This initial condition and the initial coordinates of the actual Trojan are not the same but, as they lie on the same invariant torus, they are dynamically equivalent. The choice of these initial coordinates (a^*, e^*, I^*) as proper elements of the Trojan is natural in the sense that the frequency vector is not equivalent to a trajectory but to an invariant torus. See [Robutel et al., 2005] for more details.

When we plot these Trojan “proper elements” (a^*, e^*) on the global dynamical maps for fixed inclinations I^* as just explained, we see [Robutel et al., 2005] that most of the Trojans are inside the stability region of the global maps [Michtchenko et al., 2001, Nesvorny and Dones, 2002, Tsiganis et al., 2005b] and also that some of the observed Trojans stay inside (or very close to) some of the resonances described in Section 2. This is rather easy to check when the basic frequencies of the asteroids are available. This is what we do next.

In Table 5, we show the actual Trojans that, for the SJS system, lie very close (at a distance smaller than 0.1 "/yr) to some resonance corresponding to *Family I* (see Eq. (8)), up to order 25. The first column displays the catalog number and the name of the particular asteroid. In the last column of the table, we give the distance to the exact resonance in "/yr. In the last but one column, we show the initial inclination of the particular asteroid in degrees. The remaining columns are devoted to the multiplet that defines the particular resonance inside the family.

In Section 2.3.2, we introduced the secondary three-body resonances, or *Family II* of resonances, which are due to the indirect action of Saturn to the asteroid through Jupiter. Two types of these were clearly visible in the global maps; they satisfy

$$\begin{aligned} 5\nu - 2\nu_{1,2} + pg + p_5g_5 + p_6g_6 &= 0, \quad \text{or} \\ 3\nu + \nu_{1,3} + pg + p_5g_5 + p_6g_6 &= 0, \end{aligned}$$

where recall that $\nu_{1,2} = n_5 - 2n_6$ and $\nu_{1,3} = n_5 - 3n_6$. In Table 6, we show the actual Trojans that are at a distance smaller than 0.1 "/yr of some resonance corresponding to *Family II*. Note that we group the resonant Trojans depending on the value of p . That is, we can identify subfamilies inside the different types of resonances of *Family II* to a constant p value.

In Table 7, we show some of the Trojans that are at a distance smaller than 0.1 "/yr of some representative secular resonance of *Family III* (see Eq. (12)). The computations are done up to order 14, and just a few of all the actual cases found are shown. Note that some Trojans (e.g. 5023–Agapenor, that appears in Tables 6 and 7) may even be very close to a double resonance⁴. Double resonances were already suggested as a possible explanation for the “stable chaos” of some asteroids found in [Milani, 1993] and mentioned by [Dvorak and Tsiganis, 2000], for high-order secular resonances.

In Table 8, we show some of the actual Trojans that are at a distance smaller than 0.1 "/yr of a resonance belonging to *Family IV* (see Eq. (13)). In particular, we classify them on three subfamilies depending on they satisfy $4g + \nu_{2,5} + p_5g_5 + p_6g_6 + q_6s_6 = 0$, $5g + \nu_{2,5} + p_5g_5 + p_6g_6 + q_6s_6 = 0$ or

⁴Actually, we should call them *triple resonances*, as all Trojans are already in 1:1 mean motion resonance.

Table 6: **Family II.** Some examples of actual Trojans at a distance smaller than 0.1 "/yr of one of the subfamilies of *Family II* resonances. In the last two columns, we show respectively the initial inclination of the asteroid (in degrees) and the distance to the exact resonance (in "/yr). The first table is devoted to resonances satisfying Eq. (9) and the second one Eq. (10).

$5\nu - 2\nu_{1,2} + pg + p_5g_5 + p_6g_6 + qs + q_6s_6 = 0$							
Trojan	p	p_5	p_6	q	q_6	I	dis.
23075–1999XV83	-4	-1	3	2	-2	13.0	0.004
4792–Lykaon	-3	0	3	-1	-1	8.4	0.037
3063–Makhaon	-2	-1	5	-1	-3	13.5	0.069
3564–Talthybius	-2	1	1	2	-4	15.3	0.089
5638–Deikoon	-2	4	0	1	-5	9.8	0.007
12921–1998WZ5	-2	-2	-2	-1	5	12.2	0.048
15536–2000AG191	-2	4	-4	0	0	14.7	0.035
5023–Agapenor	-1	2	-3	0	0	13.0	0.010
11554–Asios	-1	-3	2	0	0	12.5	0.093
24426–2000CR12	-1	-3	2	0	0	7.4	0.009
2893–Peiroos	0	1	-5	2	0	13.2	0.017
9817–Thersander	0	5	-7	0	0	9.0	0.026
14235–1999XA187	0	-3	3	-2	0	8.0	0.004
23119–2000AP33	0	1	1	1	-5	19.7	0.040
24275–1999XW167	0	-4	4	-2	0	13.9	0.055
3709–Polypoites	1	0	3	-7	1	19.6	0.097
5476–1989TO11	1	1	-2	2	-4	13.9	0.060
15651–Tlepolemos	1	0	3	-5	-1	2.3	0.082
17442–1989UO5	1	2	-3	-1	-1	15.3	0.056
23987–1999NB63	1	-6	3	1	-1	22.6	0.007
1873–Agenor	2	-5	1	1	-1	22.2	0.092
14268–2000AK156	2	3	-5	-2	0	16.4	0.083
22199–Klonios	2	-6	0	2	0	8.4	0.046
22222–Hodios	2	-3	1	0	-2	1.9	0.006

$3\nu + \nu_{1,3} + pg + p_5g_5 + p_6g_6 + qs + q_6s_6 = 0$							
Trojan	p	p_5	p_6	q	q_6	I	dis.
14791–Atreus	-11	10	3	0	0	3.0	0.044
11251–Icarion	-10	0	8	0	4	2.9	0.010
5284–Orsilocus	-9	3	6	-1	3	18.8	0.003
10989–Dolios	-9	4	-1	2	6	10.6	0.031
13185–1996TH52	-9	1	0	3	7	9.4	0.038
2241–Alcathous	-8	3	-1	3	5	17.8	0.007
4832–Palinurus	-8	-2	0	5	7	17.7	0.022
5023–Agapenor	-8	3	-3	7	3	13.0	0.010
7543–Prylis	-8	2	2	3	3	14.2	0.020
9907–Oileus	-8	6	4	0	0	7.4	0.045
11275–1988SL3	-8	5	5	-3	3	23.6	0.001
13383–1998XS31	-8	10	0	-1	1	7.6	0.007
13780–1998UZ8	-8	4	2	-1	5	8.0	0.039
5648–1990VU1	-7	3	-2	2	6	21.3	0.001
4791–Iphidamas	-6	7	1	0	0	27.2	0.022
5264–Telephus	-6	1	9	-1	-1	31.2	0.019
13062–Podarkes	-5	6	-5	5	1	6.6	0.011
7641–1986TT6	-4	2	6	0	-2	35.6	0.010
12444–1996GE19	-4	0	-4	11	-1	31.4	0.008
5027–Androgeos	-3	5	0	-6	6	30.2	0.028
5285–Krethon	-3	3	-6	-2	10	24.1	0.005
10247–Amphiaraos	-3	-1	0	-2	8	3.8	0.050
15663–Periphas	-3	-3	0	6	2	33.9	0.004
2363–Cebriones	-2	2	-4	0	6	32.7	0.031

Table 7: **Family III.** Some examples of actual Trojans at a distance smaller than 0.1 "/yr to a member of the secular resonances $qs + q_6s_6 + p_5g_5 + p_6g_6 = 0$, up to order 14. In the last two columns, we show the initial inclination of the asteroid (in degrees) and the distance to the exact resonance (in "/yr).

$qs + q_6s_6 + p_5g_5 + p_6g_6 = 0$						
Trojan	q	q_6	p_5	p_6	I	dis.
1173–Anchises	-5	3	4	-2	7.9	0.092
3391–Sinon	-2	2	-1	1	15.7	0.066
3451–Mentor	6	-4	-2	0	10.1	0.099
4138–Kalchas	5	-1	-6	2	2.8	0.081
5023–Agapenor	3	-3	2	-2	13.0	0.032
5126–Achaemenides	2	2	-7	3	28.3	0.065
5130–Ilioneus	6	-4	-2	0	16.9	0.061
6090–1989DJ	-1	-1	4	-2	21.4	0.013
6545–1986TR6	-5	5	-2	2	13.3	0.030
7119–Hiera	7	-5	-1	-1	20.6	0.024
7352–1994CO	-4	2	3	-1	7.0	0.026
9713–Oceax	-3	-1	7	-3	3.6	0.053
9818–Eurymachos	1	-3	5	-3	7.4	0.034
11487–1988RG10	-5	1	6	-2	4.3	0.075
11509–1990VL6	-2	0	3	-1	19.1	0.033
12054–1997TT9	5	-3	-3	1	9.4	0.062
12242–Koon	-6	2	5	-1	30.4	0.072
12929–1999TZ1	-2	0	2	0	32.3	0.009

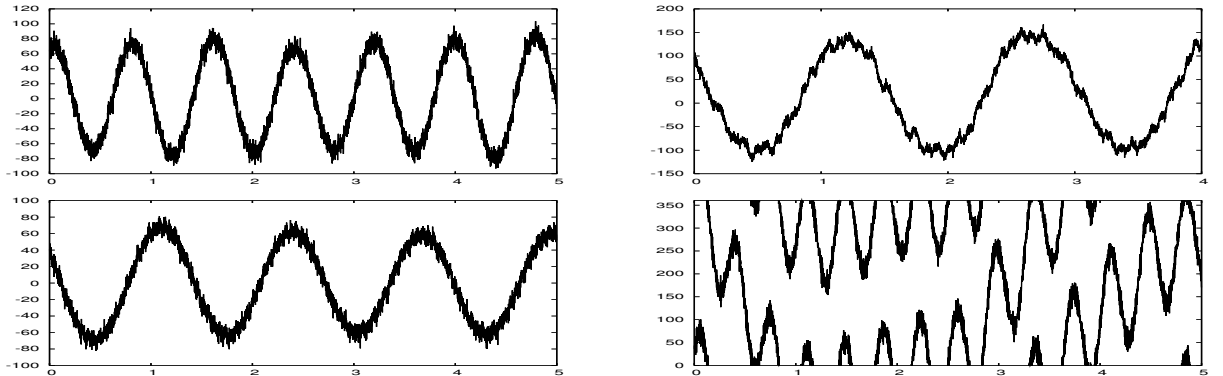


Figure 8: Evolution w.r.t. time (in Myr) of the critical angle (in degrees) of respectively, from top to bottom, 4057–Demophon, 5638–Deikoon (left column), 17423–1988SK2 and 4543–Phoinix (right column).

$6g + \nu_{2,5} + p_5g_5 + p_6g_6 + q_6s_6 = 0$. The computations are done respectively up to orders 10, 13 and 17. As it was expected from Fig. 4 and the discussion in Section 2.4, the initial inclination of the asteroids grows with the coefficient of g . We note that the initial inclination of the Trojans inside the resonances $4g$, $5g$ and $6g$ (Table 8) belongs to the intervals predicted by Fig. 4. It is also interesting to note that some asteroids (e.g. 4035–1986WD, 4057–Demophon, 5233–1988RL10, 5907–1989TU5, 17423–1988SK2 and 18228–Hyperenor) are really very close (distance smaller than 0.002 "/yr) to one of these resonances. These asteroids are actually captured inside the corresponding resonances. Indeed, we have checked that all the asteroids in Table 8 satisfying $q = q_6 = 0$ are captured by the corresponding resonances. For every particle, we have computed the evolution with respect to time of the critical angle of the corresponding resonance (see Section 3.2.1). In most of the cases, the period of libration of this critical angle inside the resonance ranges from about half to several million years (see the top three rows of Fig. 8 and Section 4.2). All these Trojans clearly follow a libration except one case: 4543–Phoinix. Even though it is very close to the exact resonance, the critical angle does not purely librate. Its motion in frequency space is close to the separatrix. See bottom frame of Fig. 8.

Some of the Trojans described above are examples of “stable chaos” (see [Milani and Nobili, 1992]). For instance, 4543–Phoinix is in stable chaos according to [Milani, 1993] and we can locate it close to the resonance $4g + \nu_{2,5} - g_5 + g_6 = 0$. See Section 4.2 for a detailed study of the long-term dynamics of this asteroid.

But not only this, 4543–Phoinix and two more Trojans (i.e., 5638–Deikoon and 17423–1988SK2), all of them lying inside the resonance $4g + \nu_{2,5} - 2g_5 + g_6 = 0$, show the displacement of this resonance in function of the initial inclination (recall Section 2.4). This resonance exits the region of stability when the inclination increases. Also, the resonance $4g + \nu_{2,5} - g_5 = 0$ follows the same evolution. Two examples of asteroids inside this latter case are: 5907–1989TU5 and 18228–Hyperenor.

A last interesting example that we want to point out is 1173–Anchises (see Table 7). This asteroid lies inside a region of overlapping and it was already in the list of “stable chaos” in [Milani et al., 1997]. It is very close to the $s = s_6$ resonance, to a resonance of *Family II* with $p = -2$, see Eq. (9), and to a secular resonance.

4.2 Long-term behavior of some observed Trojans

We now study the long-term dynamical implications of the families of resonances. They provide a mechanism for transport of actual Trojans from the inner part of the stability region to the chaotic part and, sometimes, to escaping orbits. In this paper, we shall call this diffusion mechanism Arnold-type diffusion [Arnold, 1964] and it is observed in actual Trojan asteroids. Moreover, in the numerical experiments, a second type of diffusion is also observed. This one is bounded and transversal to the secondary three-body

Table 8: **Family IV**. Actual Trojans at a distance smaller than 0.1 "/yr of a resonance of the type $4g + \nu_{2,5} + \dots = 0$, $5g + \nu_{2,5} + \dots = 0$ or $6g + \nu_{2,5} + \dots = 0$. In the last two columns, we show the initial inclination of the asteroid (in degrees) and the distance (in "/yr) to the exact resonance.

$4g + \nu_{2,5} + p_5g_5 + p_6g_6 + qs + q_6s_6 = 0$						
Trojan	p_5	p_6	q	q_6	I	dis.
2893–Peiroos	1	0	-1	-1	13.2	0.091
4035–1986WD	1	0	-1	-1	13.1	0.001
4057–Demophon	-1	0	0	0	2.8	0.002
4543–Phoinix	-2	1	0	0	16.2	0.064
4722–Agelaos	0	1	-1	-1	7.8	0.010
5123–1989BL	-3	2	0	0	7.3	0.086
5233–1988RL10	-1	0	0	0	2.5	0.0003
5638–Deikoon	-2	1	0	0	9.8	0.030
5907–1989TU5	-1	0	0	0	0.7	0.0004
9713–Oceax	-2	1	-1	1	3.6	0.007
13184–Augeias	0	-1	0	0	5.4	0.013
13463–Antiphos	0	1	-3	1	11.6	0.046
13790–1998UF31	-2	1	0	0	6.8	0.025
14518–1996RZ30	-2	1	0	0	6.2	0.026
15502–1999NV27	-1	2	0	-2	18.0	0.053
17423–1988SK2	-2	1	0	0	1.4	0.00007
18058–1999XY129	0	-1	-1	1	8.8	0.017
18228–Hyperenor	-1	0	0	0	3.2	0.002
21370–1997TB28	-1	0	1	-1	6.5	0.015
22808–1999RU12	-1	2	-2	0	9.9	0.010
24018–1999RU134	0	1	1	-3	15.2	0.085
24452–2000QU167	0	1	-2	0	6.8	0.050
$5g + \nu_{2,5} + p_5g_5 + p_6g_6 + qs + q_6s_6 = 0$						
Trojan	p_5	p_6	q	q_6	I	dis.
3596–Meriones	-1	-3	3	-1	23.8	0.060
5028–Halaesus	2	-4	-1	1	20.9	0.037
5254–Ulysses	-3	-1	1	1	22.8	0.017
5648–1990VU1	-3	-1	0	2	21.3	0.081
11887–Echemmon	-3	-1	3	-1	25.2	0.039
20424–1998VF30	-1	-1	0	0	24.4	0.050
21595–1998WJ5	0	-2	1	-1	24.0	0.045
23480–1991EL	1	-1	-2	0	23.0	0.020
$6g + \nu_{2,5} + p_5g_5 + p_6g_6 + qs + q_6s_6 = 0$						
Trojan	p_5	p_6	q	q_6	I	dis.
2363–Cebriones	-6	-1	3	1	32.7	0.029
16956–1998MQ11	-1	-4	-1	3	27.1	0.058
19844–2000ST317	1	0	2	-6	40.6	0.085
22014–1999XQ96	1	-4	-2	2	30.5	0.045

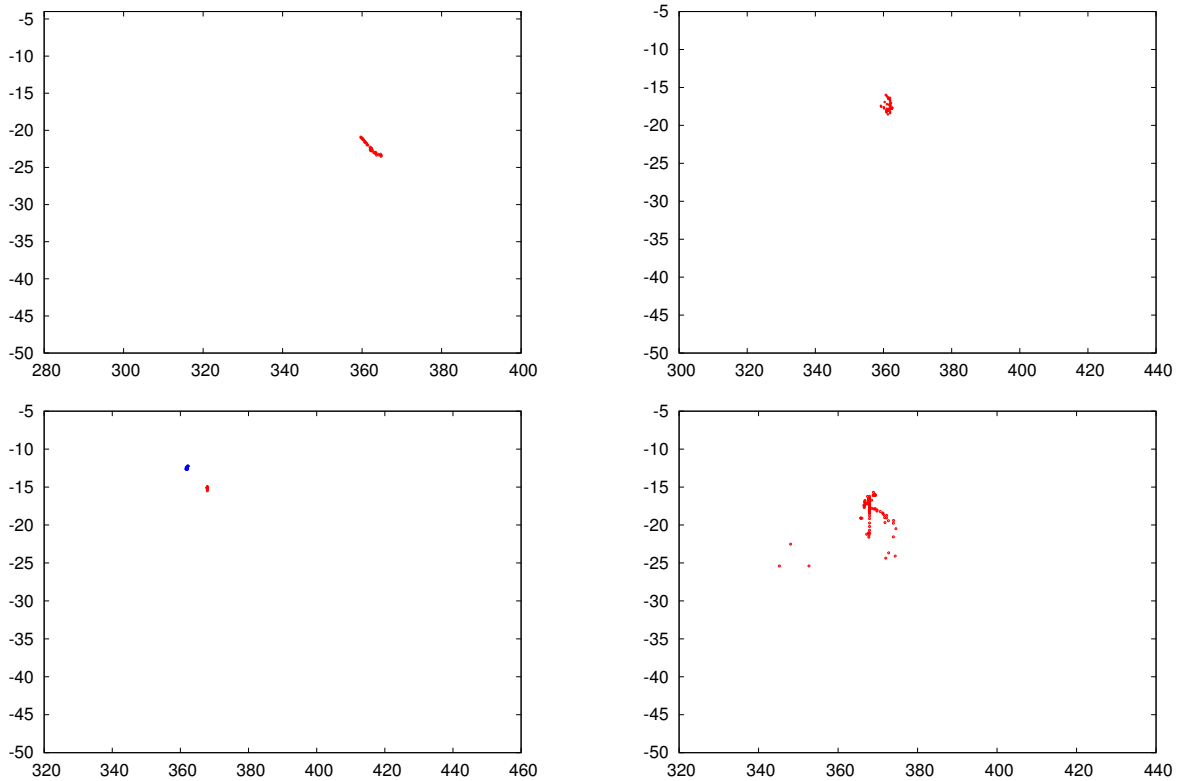


Figure 9: Diffusion along *Family IV* resonances of some actual Trojan asteroids. We show the projection of the global study into the (g, s) frequency space for four different initial inclinations. We then superimpose on these figures the evolution in time of the asteroid’s frequencies. Top-Left: 4543–Phoinix at the 16° inclination global picture. Top-Right: 5638–Deikoon at 10° inclination. Bottom-Left: 5907–1989TU5 (red) and 17423–1988SK2 (blue) at 0° inclination. Bottom-Right: 18228–Hyperenor at 4° inclination.

resonances. This reminds (see Section 3.3) a diffusion mechanism à la Chirikov [Chirikov, 1959], and thus we will call it Chirikov-type diffusion.

4.2.1 Arnold–type Diffusion

We take some asteroids from Table 8 and perform a long-term integration of their trajectories. More concretely, we take the initial conditions of 4543–Phoinix, 5638–Deikoon, 5907–1989TU5, 17423–1988SK2 and 18228–Hyperenor, and integrate them for 200 intervals of 5 Myr each. That is, we take a total time of integration of one billion years or until the asteroid escapes. For each of these intervals, we compute the basic frequencies of the Trojan (ν , g and s) to study their evolution in time. In Fig. 9, we show the results of these long-term integrations. We superimpose the (g, s) -projection of the frequencies of the particular asteroid to the corresponding global figure, that changes depending on the initial inclination.

The asteroid 4543–Phoinix starts its “journey” at the resonance $4g + \nu_{2,5} - 2g_5 + g_6 = 0$, then it is subject to a drift inside the frequency space during about 34 intervals and finally it is ejected of the stable region at approximately 170 millions years of integration time (see Fig. 9 (top-left)).

The Trojans 5638–Deikoon, close to the 10° inclination global picture, and 5907–1989TU5 and 17423–1988SK2, at 0° inclination, are transported along their corresponding resonances, but survive the billion years integration and remain in the libration region (see, respectively, Fig. 9 (top-right) and Fig. 9 (bottom-left)).

Finally, the asteroid 18228–Hyperenor does not survive the one billion years integration. It is first transported along the $4g + \nu_{2,5} - g_5 = 0$ resonance for about 500 million years, then it “travels” to the resonance $4g + \nu_{2,5} - 2g_6$, it jumps to the chaotic region and finally, after 640 million years of total integration time, it is ejected from the libration region (see Fig. 9 (bottom-right)).

4.2.2 Chirikov–type Diffusion

We now take some of the asteroids in Table 6 and study their long-term dynamics. In particular, we integrate them for one billion years and compute their basic frequencies every five million years. If we plot the evolution in time of these basic frequencies on the global (g, ν) -space, for instance, it turns out that some of these objects suffer a bounded diffusion which is pretty strong in the ν direction and weak in the g direction (see Section 3.3). Thus, in the frequency space, this diffusion is not along the resonances but transverse to them. We show some examples of these simulations in Fig. 10.

The asteroids 9817–Thersander and 11554–Asios satisfy, respectively, the resonance relations

$$\begin{aligned} 5\nu - 2\nu_{1,2} + qg_5 - (q+2)g_6 &= 0, \quad \text{with } q \in \{-8, \dots, 5\}, \\ 5\nu - 2\nu_{1,2} - g + qg_5 - (q+1)g_6 &= 0, \quad \text{with } q \in \{-7, \dots, 0\}, \end{aligned}$$

and are displayed in the top and centre frames of Fig. 10. Note how they are transported across the secondary three-body resonances suffering a large diffusion in ν . This motivates the classification made in Table 6 in subfamilies of resonances. Asteroids with a fixed p value ($p = 0$ or $p = -1$) in Eq. (9) or Eq. (10) are likely to suffer this type of diffusion by crossing resonances with different p_5 values.

Finally, in the bottom picture of Fig. 10, a very interesting example is shown: Asteroid 14791–Atreus. This asteroid suffers, during the long-term integration, transversal diffusion across the secondary three-body resonances $3\nu + \nu_{1,3} - 11g + qg_5 + (13 - q)g_6 = 0$ with $q \in \{-11, \dots, 7\}$, and, at the same time, it is transported (in frequency space) along the resonances due to the GI (or *Family IV*) and satisfies $4g + \nu_{2,5} - g_5 = 0$ or $4g + \nu_{2,5} - 2g_5 + g_6 = 0$. After approximately 825 million years, this body is ejected from the stability region.

5 Conclusions

In this paper, we have described in complete detail the resonant structure of Jupiter’s Trojan asteroids. The understanding of this global structure helps to study the Trojan stability problem in depth. We have identified four different families of resonances (classified depending on the type of frequencies involved) that have important dynamical effects: (i) The secondary resonances (*Family I* and *Family II*) generate large chaotic regions but, usually, with trapped asteroid motion; (ii) The secular resonances (*Family III*), which most important member, $s = s_6$, determines the boundary of the long-term stability region for low inclinations; and (iii) *Family IV* resonances, a new type of resonance that involves the secular frequencies and the frequency of the Great Inequality, but not the libration frequency of the asteroid, and it plays a very important dynamical role.

The existence of the first three families is not due to the direct perturbation of Saturn on the Trojans (see Section 2.3.2). Only the fourth family is generated by this direct influence. This shows that the unstable structures associated to *Family IV* are due to the overlapping of the 1:1 co-orbital resonance with Jupiter and the 2:5 mean motion resonance between the Trojan and Saturn.

Two mechanisms of diffusion have been observed in the libration region for long-term simulations (1 Gyr). One, generated by *Family II*, consists in a transversal diffusion to the secondary three-body resonances but, usually, the asteroids remain trapped near these structures. It is thus a bounded diffusion. The other takes place along *Family IV* resonances and it is crucial in the slow transport phenomenon that brings asteroids from the inner stable region to the unstable region (beyond $s = s_6$) and, often, to ejection.

In this regard, we have identified in Section 3 different paths that drive Trojans from the “inner stable regions” to the strong diffusion regions (characterized by a large overlapping of the different families of

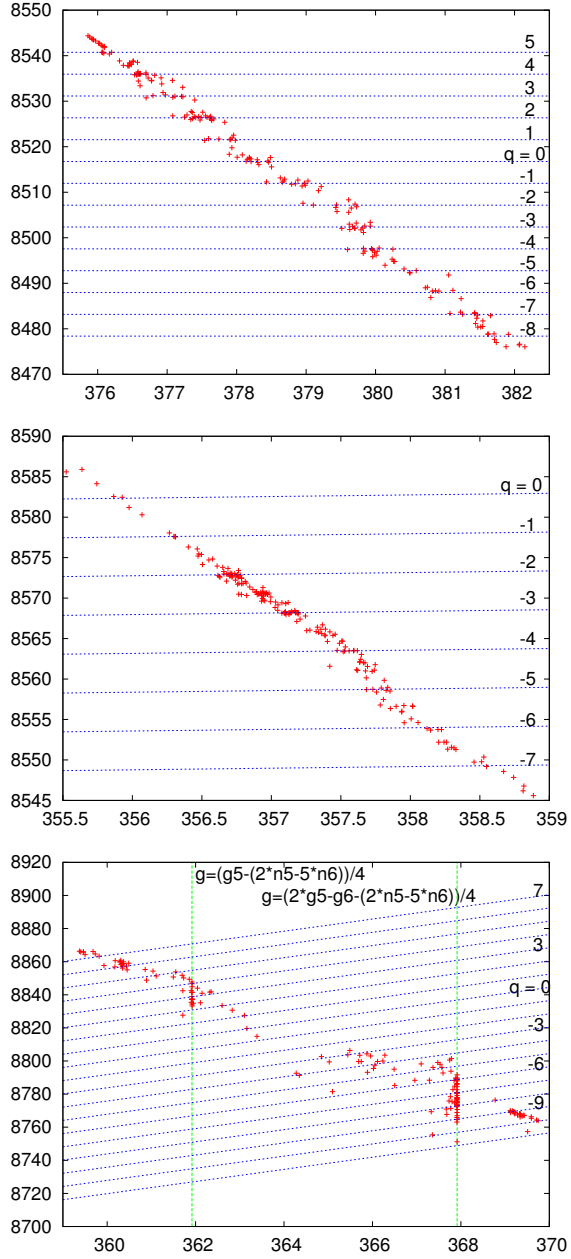


Figure 10: Chirikov diffusion transversal to the secondary three-body resonances in the (g, ν) plane of three actual Trojan asteroids. Top: 9817–Thersander, which crosses the resonances $5\nu - 2\nu_{1,2} + qg_5 - (q + 2)g_6 = 0$. Centre: 11554–Asios, which crosses the resonances $5\nu - 2\nu_{1,2} - g + qg_5 - (q + 1)g_6 = 0$. Bottom: 14791–Atreus, which crosses the resonances $3\nu + \nu_{1,3} - 11g + qg_5 + (13 - q)g_6 = 0$.

resonances), from where Trojans may be rapidly ejected. These mechanisms of global chaos (generated by the overlapping of the four families of resonance) and of slow diffusion along resonances of *Family IV* seem to be the main generator mechanisms of long-time erosion of the Trojan swarms discovered by [Levison et al., 1997]. The study of the observed Trojans, carried out in Section 4.2, shows that the structures and the mechanisms described above do really exist in nature. Indeed, Tables 5–8, and Fig. 9 and Fig. 10 give examples of asteroids trapped (temporarily or permanently) inside resonances, of bounded diffusion, and of a drift transport mechanism along resonances towards the outer unstable region.

If Trojans can be ejected from the libration region (as we have shown in this paper), following the same mechanism, there should also be possibilities of capture. In the present state of the Solar System, this mechanism of capture is far from being effective, and thus it cannot be the explanation of the formation of the Trojan swarms. Recently, [Morbidelli et al., 2005] showed that resonances between ν and $\nu_{1,2}$ generate a large chaotic behavior in the migration process just after crossing the 1:2 mean motion resonance between Jupiter and Saturn, and suggested that these events probably allowed Trojans to be captured in the co-orbital region. It is possible to generalize the families of resonances appearing in the present paper in order to model the resonant structure of the Trojans during the planetary migration course. The study of the evolution of these structures shows not only that the vicinity of the triangular Lagrangian points undergoes a sequence of relatively stable and strongly chaotic phases associated to captures and ejections, but also allows us to identify the resonances that generate this strong chaos. This mechanism, whose theoretical part is studied in a forthcoming paper [Robutel and Bodossian, 2006], seems to be very promising to tackle the remaining unanswered questions in the Trojan problem.

Acknowledgments

The authors wish to thank À. Jorba for his comments on a previous version of this manuscript. This work has been partially supported by PNP-CNRS, the MCyT/FEDER Grant BFM2003-07521-C02-01 and the CIRIT grant 2005SGR-01028. The computing clusters IBM-SP4 at CINES and Hidra at the Barcelona UB-UPC Dynamical Systems Group have been widely used.

References

- [Arnold, 1964] Arnold, V. (1964). Instability of dynamical systems with several degrees of freedom. *Soviet Math. Dokl.*, 5:581–585.
- [Beaugé and Roig, 2001] Beaugé, C. and Roig, F. (2001). A semianalytical model for the motion of the trojan asteroids: Proper elements and families. *Icarus*, 153:391–415.
- [Bien and Schubart, 1984] Bien, R. and Schubart, J. (1984). Trojan orbits in secular resonances. *Celest. Mech. Dyn. Astron.*, 34:425–434.
- [Bowell,] Bowell, E. The asteroid orbital elements database. For more information, visit <ftp://ftp.lowell.edu/pub/elgb/astorb.html>.
- [Chirikov, 1959] Chirikov, B. V. (1959). The passage of a nonlinear oscillating system through resonance. *Soviet Physics. Dokl.*, 4:390–394.
- [Chirikov, 1960] Chirikov, B. V. (1960). Resonance processes in magnetic traps. *Journal of Plasma Physics*, 1:253–260.
- [Cincotta et al., 2003] Cincotta, P. M., Giordano, C. M., and Simó, C. (2003). Phase space structure of multi-dimensional systems by means of the mean exponential growth factor of nearby orbits. *Phys. D*, 182(3-4):151–178.
- [Cincotta and Simó, 2000] Cincotta, P. M. and Simó, C. (2000). Simple tools to study global dynamics in non-axisymmetric galactic potentials - I. *Astron. Astrophys.*, 147:205–228.
- [Deprit et al., 1967] Deprit, A., Henrard, J., and Rom, A. (1967). Trojan orbits II. Birkhoff’s normalization. *Icarus*, 6:381–406.

- [Dvorak and Schwarz, 2005] Dvorak, R. and Schwarz, R. (2005). On the Stability Regions of the Trojan Asteroids. *Celest. Mech. Dyn. Astron.*, 92:19–28.
- [Dvorak and Tsiganis, 2000] Dvorak, R. and Tsiganis, K. (2000). Why do Trojan ASCs (not) Escape? *Celest. Mech. Dyn. Astron.*, 78:125–136.
- [Efthymiopoulos and Sándor, 2005] Efthymiopoulos, C. and Sándor, Z. (2005). Optimized Nekhoroshev stability estimates for the Trojan asteroids with a symplectic mapping model of co-orbital motion. *Mon. Not. Roy. Astron. Soc.*, 364:253–271.
- [Erdi, 1997] Erdi, B. (1997). The Trojan problem. *Celest. Mech. Dyn. Astron.*, 65:149–167.
- [Ferraz-Mello, 1997] Ferraz-Mello, S. (1997). A symplectic mapping approach to the study of the stochasticity in asteroidal resonances. *Celest. Mech. Dyn. Astron.*, 65:421–437.
- [Ferraz-Mello et al., 1998a] Ferraz-Mello, S., Michtchenko, T. A., and Roig, F. (1998a). High-eccentricity non-secular Three-Period Resonances inside Two-period Resonances (Kirkwood Gaps). *Bulletin of the American Astronomical Society*, 30:1028–+.
- [Ferraz-Mello et al., 1998b] Ferraz-Mello, S., Michtchenko, T. A., and Roig, F. (1998b). The Determinant Role of Jupiter’s Great Inequality in the Depletion of the Hecuba Gap. *Astron. J.*, 116:1491–1500.
- [Froeschlé et al., 1997] Froeschlé, C., Lega, E., and Gonczi, R. (1997). Fast Lyapunov indicators. Application to asteroidal motion. *Celest. Mech. Dyn. Astron.*, 67(1):41–62.
- [Gabern, 2003] Gabern, F. (2003). *On the dynamics of the Trojan asteroids*. PhD thesis, Univ. Barcelona. <http://www.maia.ub.es/dsg/2003/>.
- [Gabern and Jorba, 2004] Gabern, F. and Jorba, A. (2004). Generalizing the Restricted Three-Body Problem. The Bianular and Tricircular coherent problems. *Astron. Astrophys.*, 420:843–854.
- [Gabern and Jorba, 2005] Gabern, F. and Jorba, A. (2005). Effective computation of the dynamics around a two-dimensional torus of a Hamiltonian system. *J. Nonlinear Sci.*, 15(3):159–182.
- [Gabern et al., 2005] Gabern, F., Jorba, A., and Locatelli, U. (2005). On the construction of the Kolmogorov normal form for the Trojan asteroids. *Nonlinearity*, 18(4):1705–1734.
- [Gabern et al., 2004] Gabern, F., Jorba, A., and Robutel, P. (2004). On the accuracy of Restricted Three-Body Models for the Trojan motion. *Discrete and Continuous Dynamical Systems*, 11:751–762.
- [Giorgilli et al., 1989] Giorgilli, A., Delshams, A., Fontich, E., Galgani, L., and Simó, C. (1989). Effective stability for a Hamiltonian system near an elliptic equilibrium point, with an application to the restricted three body problem. *J. Differential Equations*, 77:167–198.
- [Giorgilli and Skokos, 1997] Giorgilli, A. and Skokos, C. (1997). On the stability of the Trojan asteroids. *Astron. Astrophys.*, 317:254–261.
- [Gomes et al., 2005] Gomes, R. S., Levison, H. F., Tsiganis, K., and Morbidelli, A. (2005). Origin of the cataclysmic Late Heavy Bombardment period of the terrestrial planets. *Nature*, 435:466–469.
- [Gómez et al., 2001] Gómez, G., Jorba, À., Simó, C., and Masdemont, J. (2001). *Dynamics and mission design near libration points. Vol.IV*, volume 5 of *World Scientific Monograph Series in Mathematics*. World Scientific Publishing Co. Inc., River Edge, NJ. Advanced methods for triangular points.
- [Grazier et al., 1999a] Grazier, K. R., Newman, W. I., Kaula, W. M., and Hyman, J. M. (1999a). Dynamical Evolution of Planetesimals in the Outer Solar System. I. The Jupiter/Saturn Zone. *Icarus*, 140:341–352.
- [Grazier et al., 1999b] Grazier, K. R., Newman, W. I., Varadi, F., Kaula, W. M., and Hyman, J. M. (1999b). Dynamical Evolution of Planetesimals in the Outer Solar System. II. The Saturn/Uranus and Uranus/Neptune Zones. *Icarus*, 140:353–368.
- [Guzzo, 2005] Guzzo, M. (2005). The web of three-planet resonances in the outer solar system. *Icarus*, 174:273–284.
- [Jorba and Villanueva, 1997] Jorba, À. and Villanueva, J. (1997). On the persistence of lower dimensional invariant tori under quasi-periodic perturbations. *J. Nonlinear Sci.*, 7:427–473.

- [Laskar, 1990] Laskar, J. (1990). The chaotic motion of the Solar System. A numerical estimate of the size of the chaotic zone. *Icarus*, 88:266–291.
- [Laskar, 1999] Laskar, J. (1999). Introduction to frequency map analysis. In Simó, C., editor, *Hamiltonian Systems with Three or More Degrees of Freedom*, NATO ASI, pages 134–150. Kluwer, Dordrecht.
- [Laskar, 2003] Laskar, J. (2003). Frequency map analysis in particle accelerators. In Chew, J., Lucas, P., and Webber, S., editors, *2003 Particle Accelerator Conference*, pages 378–382. IEEE, Portland.
- [Laskar, 2005] Laskar, J. (2005). Frequency map analysis and quasiperiodic decomposition. In Benest, D., editor, *Hamiltonian systems and Fourier analysis : new prospects for gravitational dynamics*, Advances in astronomy and astrophysics, pages 99–129. Cambridge Scientific Publishers.
- [Laskar and Robutel, 2001] Laskar, J. and Robutel, P. (2001). High order symplectic integrators for perturbed Hamiltonian systems. *Celest. Mech. Dyn. Astron.*, 80:39–62.
- [Lega et al., 2003] Lega, E., Guzzo, M., and Froeschlé, C. (2003). Detection of Arnold diffusion in Hamiltonian systems. *Phys. D*, 182(3-4):179–187.
- [Lemaitre and Henrard, 1990] Lemaitre, A. and Henrard, J. (1990). On the origin of the chaotic behavior in the 2/1 Kirkwood gap. *Icarus*, 32:390–.
- [Levison et al., 1997] Levison, H., Shoemaker, E., and Shoemaker, C. (1997). The long-term dynamical stability of Jupiter’s Trojan asteroids. *Nature*, 385:42–44.
- [Marzari and Scholl, 2002] Marzari, F. and Scholl, H. (2002). On the Instability of Jupiter’s Trojans. *Icarus*, 159:328–338.
- [Michtchenko et al., 2001] Michtchenko, T., Beaugé, C., and Roig, F. (2001). Planetary migration and the effects of mean motion resonances on Jupiter’s Trojan asteroids. *Astron. J.*, 122:3485–3491.
- [Milani, 1993] Milani, A. (1993). The Trojan asteroid belt: proper elements, stability, chaos and families. *Celest. Mech. Dyn. Astron.*, 57:59–94.
- [Milani and Nobili, 1992] Milani, A. and Nobili, A. M. (1992). An example of stable chaos in the Solar System. *Nature*, 357:569–571.
- [Milani et al., 1997] Milani, A., Nobili, A. M., and Knezevic, Z. (1997). Stable chaos in the asteroid belt. *Icarus*, 125:13–31.
- [Morais, 2001] Morais, M. H. M. (2001). Hamiltonian formulation of the secular theory for Trojan-type motion. *Astron. Astrophys.*, 369:677–689.
- [Morbidelli, 2002] Morbidelli, A. (2002). *Modern celestial mechanics : aspects of solar system dynamics*. Taylor & Francis, London, 2002, ISBN 0415279399.
- [Morbidelli et al., 2005] Morbidelli, A., Levison, H. F., Tsiganis, K., and Gomes, R. S. (2005). Chaotic capture of Jupiter’s Trojan asteroids in the early Solar System. *Nature*, 435:462–465.
- [Nesvorny and Dones, 2002] Nesvorny, D. and Dones, L. (2002). How long-live are the hypothetical Trojan populations of Saturn, Uranus, and Neptune? *Icarus*, 160:271–288.
- [Nesvorny et al., 2002] Nesvorny, D., Thomas, F., Ferraz-Mello, S., and Morbidelli, A. (2002). A perturbative treatment of the co-orbital motion. *Celest. Mech. Dyn. Astron.*, 82:323–361.
- [Robutel, 2005] Robutel, P. (2005). Frequency analysis and global dynamics of a planetary system. In Benest, D., editor, *Hamiltonian systems and Fourier analysis : new prospects for gravitational dynamics*, Advances in astronomy and astrophysics, pages 179–198. Cambridge Scientific Publishers.
- [Robutel and Bodossian, 2006] Robutel, P. and Bodossian, J. (2006). The resonant structure of Jupiter’s Trojan asteroids II: Evolution during the planetary migration. Preprint.
- [Robutel et al., 2005] Robutel, P., Gabern, F., and Jorba, A. (2005). The observed Trojans and the global dynamics around the lagrangian points of the Sun-Jupiter system. *Celest. Mech. Dyn. Astron.*, 92:53–69.

- [Robutel and Laskar, 2000] Robutel, P. and Laskar, J. (2000). Global dynamics in the Solar System. In Pretka-Ziomek, H., Wnuk, E., Seidelmann, P. K., and Richardson, D., editors, *Dynamics of Natural and Artificial Celestial Bodies*, pages 253–258. US/European Celestial Mechanics Workshop, Kluwer Academic Publishers.
- [Robutel and Laskar, 2001] Robutel, P. and Laskar, J. (2001). Frequency map and global dynamics in the Solar System I. *Icarus*, 152:4–28.
- [Sandor and Erdi, 2003] Sandor, Z. and Erdi, B. (2003). Symplectic mappings for Trojan-type motion in the elliptic restricted three-body problem. *Celest. Mech. Dyn. Astron.*, 86:301–319.
- [Sandor et al., 2002] Sandor, Z., Erdi, B., and Murray, C. (2002). Symplectic mappings of co-orbital motion in the restricted problem of three bodies. *Celest. Mech. Dyn. Astron.*, 84:355–368.
- [Simó, 1989] Simó, C. (1989). Estabilitat de sistemes Hamiltonians. *Mem. Real Acad. Cienc. Artes Barcelona*, 48(7):303–348.
- [Simó et al., 1995] Simó, C., Gómez, G., Jorba, À., and Masdemont, J. (1995). The Bicircular model near the triangular libration points of the RTBP. In Roy, A. and Steves, B., editors, *From Newton to Chaos*, pages 343–370, New York. Plenum Press.
- [Skokos et al., 2004] Skokos, C., Antonopoulos, C., Bountis, T. C., and Vrahatis, M. N. (2004). Detecting order and chaos in Hamiltonian systems by the SALI method. *J. Phys. A*, 37(24):6269–6284.
- [Tsiganis et al., 2000] Tsiganis, K., Dvorak, R., and Pilat-Lohinger, E. (2000). Thersites: a ‘jumping’ Trojan? *Astron. Astrophys.*, 354:1091–1100.
- [Tsiganis et al., 2005a] Tsiganis, K., Gomes, R. S., Morbidelli, A., and Levison, H. F. (2005a). Origin of the orbital architecture of the giant planets of the Solar System. *Nature*, 435:459–461.
- [Tsiganis et al., 2005b] Tsiganis, K., Varvoglis, H., and Dvorak, R. (2005b). Chaotic diffusion and effective stability of Jupiter Trojans. *Celest. Mech. Dyn. Astron.*, 92:71–87.
- [Yoder, 1979] Yoder, C. (1979). Notes on the origin of the Trojan asteroids. *Icarus*, 40:341–344.

Appendix

The linear secular approximation: Elliptic Restricted Three-Body Problem

In the planar ERTBP, the elliptic elements of the triangular equilibrium point L_4 are equal to: $a = a_5$, $\lambda = \lambda_5 + \pi/3$, $e = e_5$ and $\varpi = \varpi_5 + \pi/3$. In this case, it is useful to expand the Hamiltonian w.r.t. the quantities $\delta = (a - a_5)/a_5$, $\sigma_\nu = \lambda - \lambda_5 - \pi/3$, $z = e \exp i\varpi$ and $z_5 = e_5 \exp i\varpi_5$ in a neighborhood of L_4 , to consider its second degree terms (linear terms) and to average with respect the fast angle λ_5 (see [Morais, 2001]). Then, the secular quadratic part of the ERTBP Hamiltonian can be written as:

$$H = -\frac{3}{8}n_5^2 a_5^2 (\delta^2 + 3\varepsilon\sigma_\nu^2) - \frac{27}{16}\varepsilon n_5^2 a_5^2 (z - z_5 \exp(i\pi/3)) (\bar{z} - \bar{z}_5 \exp(-i\pi/3)), \quad (28)$$

where $\varepsilon = m_5/(m_0 + m_5)$ and, m_0 and m_5 are respectively the masses of Sun and Jupiter.

Now, we are going to perform a sequence of canonical changes of variables to Hamiltonian (28) to simplify it as much as possible. Let us start by using the canonical variables $(\sigma_\nu, S, x, -i\bar{x})$, that are defined as

$$S = \Lambda_5(\sqrt{1 + \delta} - 1), \quad \Lambda_5 = \sqrt{\mu a_5} \quad \text{and} \quad z = x \sqrt{\frac{2}{\Lambda_5} \left(1 - \frac{x\bar{x}}{2\Lambda_5}\right)}, \quad (29)$$

where $\mu = G(m_0 + m_5)$. Then, (28) becomes

$$H = -\frac{3}{8}n_5^2 a_5^2 \left(\left(\frac{2S}{\Lambda_5}\right)^2 + (\sqrt{3\varepsilon}\sigma_\nu)^2 \right) - \frac{27}{8}\varepsilon n_5 \left(x - z_5 \exp(i\pi/3) \sqrt{\frac{\Lambda_5}{2}} \right) \left(\bar{x} - \bar{z}_5 \exp(-i\pi/3) \sqrt{\frac{\Lambda_5}{2}} \right). \quad (30)$$

The second change of variables that we perform is defined by

$$S = (\sqrt{3\varepsilon}\Lambda_5/2)^{1/2}u, \quad \sigma_\nu = (\sqrt{3\varepsilon}\Lambda_5/2)^{-1/2}v, \quad y = x - z_5 \sqrt{\Lambda_5/2} \exp(i\pi/3) \approx \sqrt{\Lambda_5/2}(z - z_5 \exp(i\pi/3)). \quad (31)$$

In this case, the Hamiltonian (30) simplifies to

$$H = \nu_0 \frac{u^2 + v^2}{2} + g_0 y \bar{y}, \quad (32)$$

with $\nu_0 = \sqrt{(27\varepsilon/4)}n_5$ and $g_0 = (27/8)\varepsilon n_5$.

From this linear dynamics, it is easy to derive Eqs. (2). Also, the identity in Eq. (3) is obtained from the fact that $u^2 + v^2$ is constant. Finally, if we define the ‘‘linear’’ action-angle variables $(I_\nu, I_g, \theta_\nu, \theta_g)$ as

$$u - iv = \sqrt{2I_\nu} \exp(i\theta_\nu), \quad y = \sqrt{I_g} \exp(i\theta_g), \quad (33)$$

the Hamiltonian (32) becomes:

$$H = \nu_0 I_\nu + g_0 I_g. \quad (34)$$

In the first order approximation, these ‘‘linear’’ actions can be written in terms of the original coordinates as

$$I_\nu \approx \frac{\Lambda_5}{4\sqrt{3\varepsilon}} (\delta^2 + 3\varepsilon\sigma_\nu^2) \quad I_g \approx \frac{\Lambda_5}{2} (e^2 + e_5^2 - 2ee_5 \cos \sigma_g) = \frac{\Lambda_5}{2} ((e - e_5 \cos \sigma_g)^2 + e_5^2 \sin^2 \sigma_g), \quad (35)$$

where $\sigma_g = \varpi - \varpi_5 - \pi/3$. Therefore, it is clear from this linear approximation that, at least in a neighborhood of L_4 , the phase space should be symmetric with respect to the lines $a = a_5$ and $e = e_5 \cos \sigma_g$ (if $\cos \sigma_g > 0$). See Section 2.3.1.

The linear secular approximation: Quasi-Periodic Models

For the ERTBP, the quantity z_5 is constant. But for more general models (e.g. some of the models considered in Section 2.3), z_5 is a quasi-periodic function of time. Thus, in this case, the transformation (31) is time-dependent and it should be modified in order to normalize and autonomize the quadratic part of the secular Hamiltonian (28) to the normal form (34) (see [Gabern and Jorba, 2005]).

If we assume the quasi-periodic decomposition of z_5 (see Table 2), we can expand it in Fourier series as

$$z_5 = \sum_j \alpha_j \exp(if_j t). \quad (36)$$

In this case, the transformation (31) should be replaced by

$$y = x - g_0 \sqrt{\Lambda_5/2} \sum_j \frac{\alpha_j}{g_0 - f_j} \exp(if_j t + i\pi/3) \approx \sqrt{\Lambda_5/2} \left(z - g_0 \sum_j \frac{\alpha_j}{g_0 - f_j} \exp(if_j t + i\pi/3) \right). \quad (37)$$